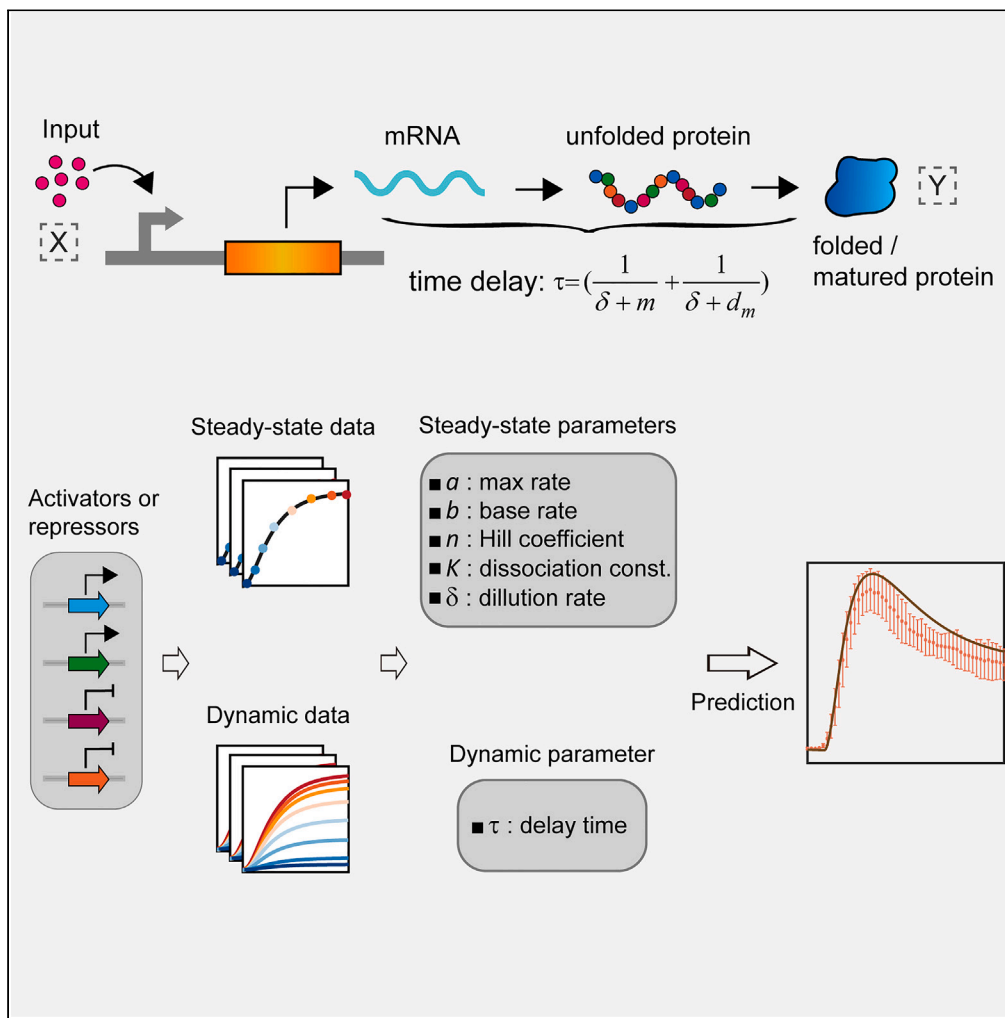# iScience

Article

The dynamic-process characterization and prediction of synthetic gene circuits by dynamic delay model

Yanhong Sun,
Fengyu Zhang, Qi
Ouyang,
Chunxiong Luo

zhangfengyu@ucas.ac.cn (F.Z.)
pkuluocx@pku.edu.cn (C.L.)

Highlights

The dynamic delay model
(DDM)

The dynamic determining
part and the doses-related
steady-state-determining
part

The detail formula of the
dynamic determining
function

Dynamic prediction of
synthetic circuits using
DDM

Article

The dynamic-process characterization and prediction of synthetic gene circuits by dynamic delay model

Yanhong Sun,[1,2] Fengyu Zhang,[3,*] Qi Ouyang[1,2] and Chunxiong Luo[1,2,3,4,*]

SUMMARY

Differential equation models are widely used to describe genetic regulations, predict multicomponent regulatory circuits, and provide quantitative insights. However, it is still challenging to quantitatively link the dynamic behaviors with measured parameters in synthetic circuits. Here, we propose a dynamic delay model (DDM) which includes two simple parts: the dynamic determining part and the doses-related steady-state-determining part. The dynamic determining part is usually supposed as the delay time but without a clear formula. For the first time, we give the detail formula of the dynamic determining function and provide a method for measuring all parameters of synthetic elements (include 8 activators and 5 repressors) by microfluidic system. Three synthetic circuits were built to show that the DDM can notably improve the prediction accuracy and can be used in various synthetic biology applications.

INTRODUCTION

Cells control gene expression by regulating the production of specific gene products, which is vital for cells to respond to a variety of intra- and extracellular signals.[1–3] The temporal dynamics of a wide range of different circuits are important for cells to adapt to complicated environments.[1,2,4–7] Synthetic biology provides a bottom-up approach to understanding complex gene regulation in nature[8,9] and engineering cell systems for novel applications. Although synthetic biology technology has been successfully used to achieve high-quality compound production,[10] cell-based toxic biosensors[11,12] and other functions,[13] many problems still need to be addressed to realize more applications.[14,15] One important problem is the quantitative prediction of synthetic circuits with mathematical models.[14,16]

To date, some mathematical models have been applied to guide the design of complicated synthetic gene circuits,[8,14,17–20] such as Hill-type functions[21–25] and other ordinary differential equation (ODE) models.[26,27] To quantitatively predict the behavior of synthetic genetic circuits, most researchers use doses related Hill-type functions[24] to fit experimental data to determine the parameters; however, these methods consider only the protein production step and do not consider the transcription, translation, or folding/maturation of proteins.[21,28,29] The lack of details about some gene expression processes may help to reduce the number of parameters while obtaining the main circuit properties in some circumstances, such as dose-response prediction for synthetic circuits.[21,28] However, for other circumstances, those details may have significant influences on the prediction of the dynamic behaviors of genetic circuits.

Transcription-translation processes may be completed in different times by various species in different environments.[30–33] Moreover, protein maturation may cause a significant time delay when fluorescent proteins are used to represent the expression of the target gene.[34] In fact, the protein folding times of most proteins in prokaryotes and eukaryotes cannot be measured with existing methods. For most of the proteins in biological systems, reasonable folding times may be about 10 min, which is comparable to the timescale of transcription and mRNA degradation.[35,36] These time delays caused by transcription-translation processes might significantly affect the behaviors of multistep induction circuits, adaptation circuits,[3,6,24] oscillators,[23,25,37–39] and circadian rhythm-related regulation processes.[40–42]

Thus, detailed models, which include inducer binding, transcription, translation and protein folding/maturation, need at least three to four ODEs.[25,43–45] In this circumstance, too many parameters need to be characterized based on the results of limited experiments, which may result in overfitting or multiple groups of parameters meeting the requirements. Delay differential equations (DDEs) are proposed to simplify the multistep reactions into a single time delay, which may reduce the number of parameters that are needed to predict dynamic

[1]The State Key Laboratory for Artificial Microstructures and Mesoscopic Physics, School of Physics, Peking University, Beijing 100871, China
[2]Center for Quantitative Biology, Academy for Advanced Interdisciplinary Studies, Peking University, Beijing 100871, China
[3]Wenzhou Institute University of Chinese Academy of Sciences, Wenzhou, Zhejiang 325001, China
[4]Lead contact
*Correspondence: zhangfengyu@ucas.ac.cn (F.Z.), pkuluocx@pku.edu.cn (C.L.)
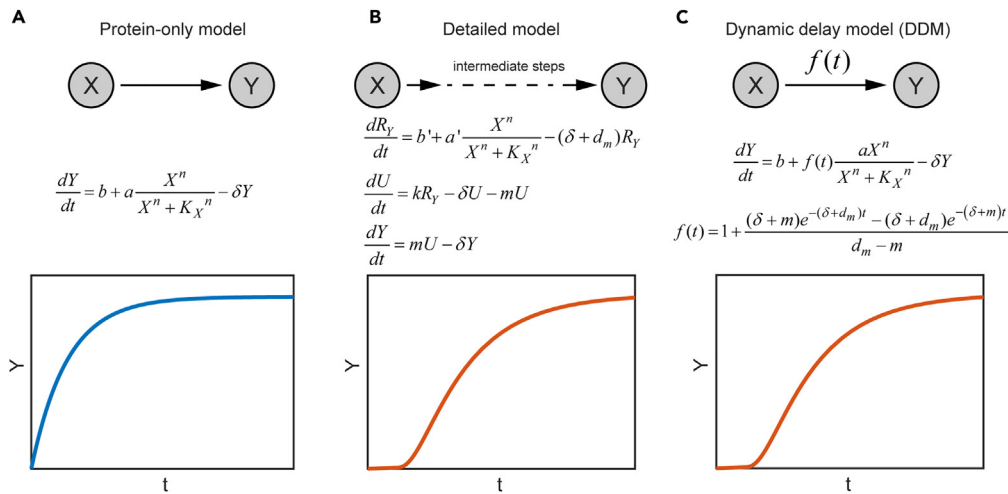https://doi.org/10.1016/j.isci.2024.109142

Figure 1. The simplest one-step regulation circuit showed an obvious time delay when intermediate steps were added, and the time delay can be described by a delay function $f(t)$

(A) Illustration of the one-step regulation circuit and the protein-only model without consideration of the transcription-translation processes. When the transcription-translation processes were not considered, the simulation increased quickly immediately after the addition of input *X*.

(B) Illustration of the one-step regulation circuit with the intermediate steps and the detailed model. The detailed model describes each of the intermediate steps with an ODE. When the intermediate steps are considered, the simulation shows an obvious time shift compared with the protein-only model.

(C) Illustration of the one-step regulation circuit and the DDM with $f(t)$ describing the time delay caused by the transcription-translation processes. The simulation results of the DDM are the same as those of the detailed model.

behaviors.[46–52] DDEs for modeling gene expression have been proposed in many works to study the influences of delays in gene expression networks,[53–56] or predict experimental behaviors of lac operon dynamics.[55] The methods of introducing delay time in these works can be summarized as follows: (1) Directly assume a total delay time τ without the precise formula link to the detailed model[53,54]; (2) Consider a delay time at each step of transcription, translation and protein folding/maturation.[55,56] The first method was simple and convenient for theoretical analysis of influences of delay times, but how specific parameters in detailed model affects the delay time was still not clear. The second method showed how to calculate the delay times in each step of transcription, translation and protein folding/maturation, but with many parameters need to be determined if it is used to predict synthetic gene expression dynamics. All methods were little used in synthetic gene units' characterization and gene circuits performance predictions.

Here, we developed a mathematical approach to link the detailed model to a new DDE model which consists the dynamic determining part (delay function), and the doses-related steady-state-determining part. The model we developed here was called the dynamic delay model (DDM). In the mathematical derivation, we aimed to determine the actual delay function of basic synthetic elements in living cells. After verified by experiment, our DDM could be used to derive the delay function of regulatory proteins in experiments. After determining the delay times and dose-determined steady-state-parameters of regulatory proteins (including activators and repressors), we used the model to predict cascaded repression circuits and incoherent feedforward loop (IFFL) networks,[3,24,28] proving that our model can be used to precisely predict synthetic network dynamics.

RESULTS

DDM

We started with a transcriptional regulation model for the simplest one-step regulation processes (Figure 1A, left). The input *X* controls the expression of protein *Y*. Here, *X* is supposed as a continuous inducer input. When the detailed steps are ignored and only the production of protein is considered, the commonly used ODE model is formulated as follows[28]:

$$\frac{dY}{dt} = b + a\frac{X^n}{X^n + K_X{}^n} - \delta Y \qquad \text{(Equation 1)}$$

where *b* and *a* are the basal and maximum production rates of protein *Y*, respectively, K_X is the dissociation constant, *n* is the Hill coefficient reflecting the cooperativity of the activators, and *δ* is the dilution rate due to cell division. We call the above model the protein-only model.

When the intermediate steps are not considered, protein *Y* starts to accumulate immediately after input *X* is added, and the protein concentration gradually increases until it plateaus over time (Figure 1A).

When processes such as transcription, translation and protein folding/maturation are considered, the detailed ODE model should be written as[47] (Figure 1B):

$$\frac{dR_Y}{dt} = b' + a'\frac{X^n}{X^n + K_X{}^n} - (\delta + d_{m_Y})R_Y$$

$$\frac{dU}{dt} = k_Y R_Y - \delta U - m_Y U \qquad \text{(Equation 2)}$$

$$\frac{dY}{dt} = m_Y U - \delta Y$$

where R_Y is the mRNA concentration, b' and a' are the basal and maximal transcription rates, K_X is the dissociation constant, n is the Hill coefficient, and d_{m_Y} is the mRNA decay rate. Here, U is the unfolded protein, and Y is the folded (e.g., regulatory proteins) or matured (e.g., fluorescent proteins) protein, k_Y is the translation rate, and m_Y is the protein folding/maturation rate. The above model is termed the detailed model.

When the transcription, translation and protein folding/maturation steps are added, the initial expression of protein Y increases more slowly than in the previous protein-only model (Figure 1B).

Moreover, this system can be transformed into a third-order ODE as follows:

$$\frac{d^3Y}{dt^3} = m_Y k_Y b' + m_Y k_Y a'\frac{X^n}{X^n + K_X{}^n} - (3\delta + d_{m_Y} + m_Y)\frac{d^2Y}{dt^2} - (3\delta^2 + 2\delta m_Y + 2\delta d_{m_Y} + m_Y d_{m_Y})\frac{dY}{dt} - \delta(\delta + m_Y)(\delta + d_{m_Y})Y$$

(Equation 3)

With eigenvalues as follows:

$$\lambda_1 = -\delta, \lambda_2 = -(\delta + m_Y), \lambda_3 = -(\delta + d_{m_Y}) \qquad \text{(Equation 4)}$$

Then, formulas for Y and $\frac{dY}{dt}$ can be derived as follows:

$$Y(t) = \sum_{i=1}^{3} C_i e^{\lambda_i t} + \frac{(1 - e^{-\delta t})}{\delta m_Y d_{m_Y}}\left[m_Y k_Y b' + m_Y k_Y a'\frac{X^n}{X^n + K_X{}^n}\right] - \frac{(1 - e^{-(\delta + m_Y)t})}{m_Y(d_{m_Y} - m_Y)(\delta + m_Y)}\left[m_Y k_Y b' + m_Y k_Y a'\frac{X^n}{X^n + K_X{}^n}\right]$$
$$+ \frac{(1 - e^{-(\delta + d_{m_Y})t})}{d_{m_Y}(d_{m_Y} - m_Y)(\delta + d_{m_Y})}\left[m_Y k_Y b' + m_Y k_Y a'\frac{X^n}{X^n + K_X{}^n}\right]$$

(Equation 5)

Here, Y should have the same steady-state concentration as in Equation 1 (STAR Methods):

$$Y_s = \frac{m_Y k_Y}{\delta(\delta + d_{m_Y})(\delta + m_Y)}\left(b' + a'\frac{X^n}{X^n + K_X{}^n}\right) = \frac{b}{\delta} + \frac{a}{\delta}\frac{X^n}{X^n + K_X{}^n} \qquad \text{(Equation 6)}$$

Then the relation between a' (b') and a (b) can be determined as follows:

$$a = \frac{m_Y k_Y a'}{(\delta + m_Y)(\delta + d_{m_Y})}, b = \frac{m_Y k_Y b'}{(\delta + m_Y)(\delta + d_{m_Y})} \qquad \text{(Equation 7)}$$

Then, the three equations representing the detailed model can be transformed into one ODE with a delay function, as follows (Figure 1B):

$$\frac{dY}{dt} = b + f(t)\frac{aX^n}{X^n + K_X} - \delta Y \qquad \text{(Equation 8)}$$

where the delay function is as follows:

$$f(t) = 1 + \frac{(\delta + m_Y)e^{-(\delta + d_{m_Y})t} - (\delta + d_{m_Y})e^{-(\delta + m_Y)t}}{d_{m_Y} - m_Y} \qquad \text{(Equation 9)}$$

When $t = 0$, which refers to the steady state before adding X, $f(0) = 0$. And when $t \to \infty$, which refers to the steady state after the onset of gene regulation with the effect of X, $f(\infty) \to 1$. Here, $f(t)$ is a function that starts at zero and gradually increases to the unit one over time. When $f(t) = 1$, the equation is the same with the protein-only model. While other parameters are the same with the protein-only model which can be determined by the dose-response curve.

We call the above model the DDM. This model is derived without approximations and can completely replace the detailed model presented above. The simulation of this model is the same as that of the detailed model with the same increasing behavior, which is different from the behavior of the protein-only model (Figure 1C). But the parameters in the DDM model are much easier to be determined by experiment data than the detailed model for the DDM model has the same doses-related steady-state-determining part with the protein-only model.
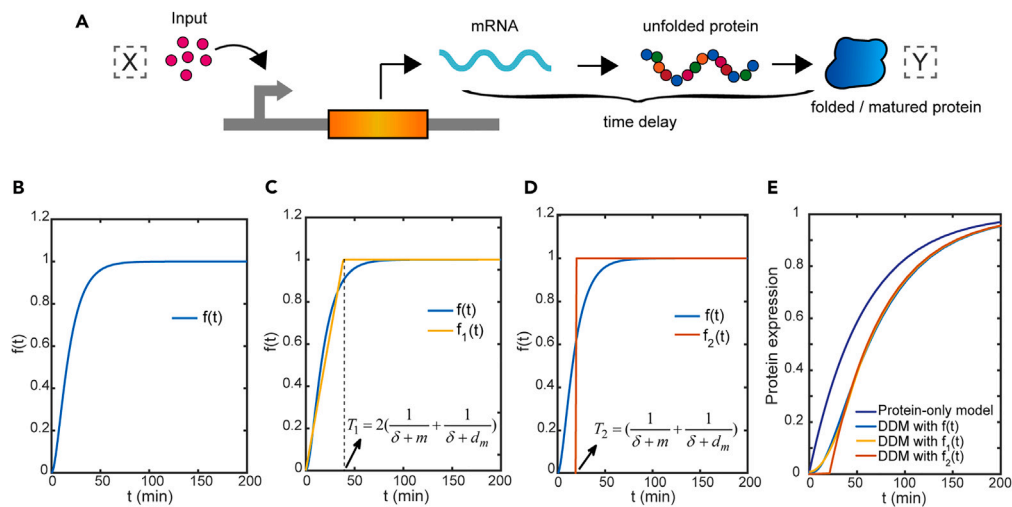
Figure 2. Simulation of $f(t)$ and its approximations

(A) Illustration of transcription-translation processes that result in a time delay.

(B) Simulation of $f(t)$.

(C) Comparison of the simulation results of $f(t)$ and $f_1(t)$.

(D) Comparison of the simulation results of $f(t)$ and $f_2(t)$.

(E) Simulations of the expression level of protein Y after the addition of a continuous unchangeable input X using the protein-only model and DDMs with $f(t)$, $f_1(t)$, and $f_2(t)$.

Determining the delay time with the delay function

The DDM has the same steady state as the protein-only model, which means that the two models have the same doses-related steady-state-determining parameters (Equation 1; Equation 8). The time delay caused by transcription-translation processes (Figure 2A) can be described by the delay function $f(t)$ in the DDM, and $f(t)$ gradually increases over time until it reaches a value of 1 (Figure 2B). Therefore, one important property of the DDM is that the dynamic determining part can be separated from the doses-related steady-state-determining part, which means that the doses-related steady-state-determining parameters can be derived based on the dose-response data, while the dynamic related parameters can be derived based on the dynamic response data. The dynamic determining part is related to the mRNA decay rate d_{m_Y}, the protein folding/maturation rate m_Y and the cell division rate δ (Equation 9).

Since the doses-related steady-state-determining parameters can be derived by fitting the dose-response data, the remaining problem is determining the dynamic related parameters in $f(t)$. The most common and direct method is to fit the experimental data based on $f(t)$; with this approach, only two parameters (m_Y and d_{m_Y}) need to be determined, as the cell division rate δ can be derived based on time-lapse micrograph data.[57] The position of d_m and m in the formula of $f(t)$ is symmetric, when the values of d_m and m are exchanged, the value of $f(t)$ is the same. Here, we provided ranges for m_Y and d_{m_Y}, and then calculated the R-squared value by fitting the LacI-GFP experimental $f(t)$ data (Figure S1A). The ranges of m_Y and d_{m_Y} were both $0\sim1$ min^{-1}, which indicated that the ranges of the half-maturation and half-decay times were both $\ln 2 \rightarrow \infty$ min. The R-squared value showed that multiple parameter values satisfied the maximum R-squared, which meant that no certain value could be determined with this method. This situation might be due to the parameter symmetry of $f(t)$ (Equation 9). Since both the protein folding/maturation rate (m_Y) and the mRNA decay rate (d_{m_Y}) can be different in different species,[30–36] neither m_Y nor d_{m_Y} can be ignored in $f(t)$. As direct fitting was not applicable, we proposed two approximation methods: a linear approximation of $f(t)$ (Figure 2C) and a step function approximation (Figure 2D), which could be matched to a DDE. We proved that $f(t) \approx 1$ when

$$t = 2\left(\frac{1}{\delta+m_Y} + \frac{1}{\delta+d_{m_Y}}\right)$$

(Equation 10)

With this approach, we could approximate $f(t)$ with a piecewise function (for more details, see STAR Methods):

$$f_1(t) = \begin{cases} \dfrac{t}{T_1} & t < T_1 \\ 1 & t \geq T_1 \end{cases} \qquad T_1 = 2\left(\frac{1}{\delta+m_Y} + \frac{1}{\delta+d_{m_Y}}\right)$$

(Equation 11)

A comparison of the simulation results of $f(t)$ and $f_1(t)$ is shown in Figure 2C.

When the input X is a continuous inducer without any changes, the linear approximation of $f(t)$ is useful. However, when the input changes, such as a periodic addition function, the linear approximation may be difficult to use. Therefore, we proposed another approximation, the
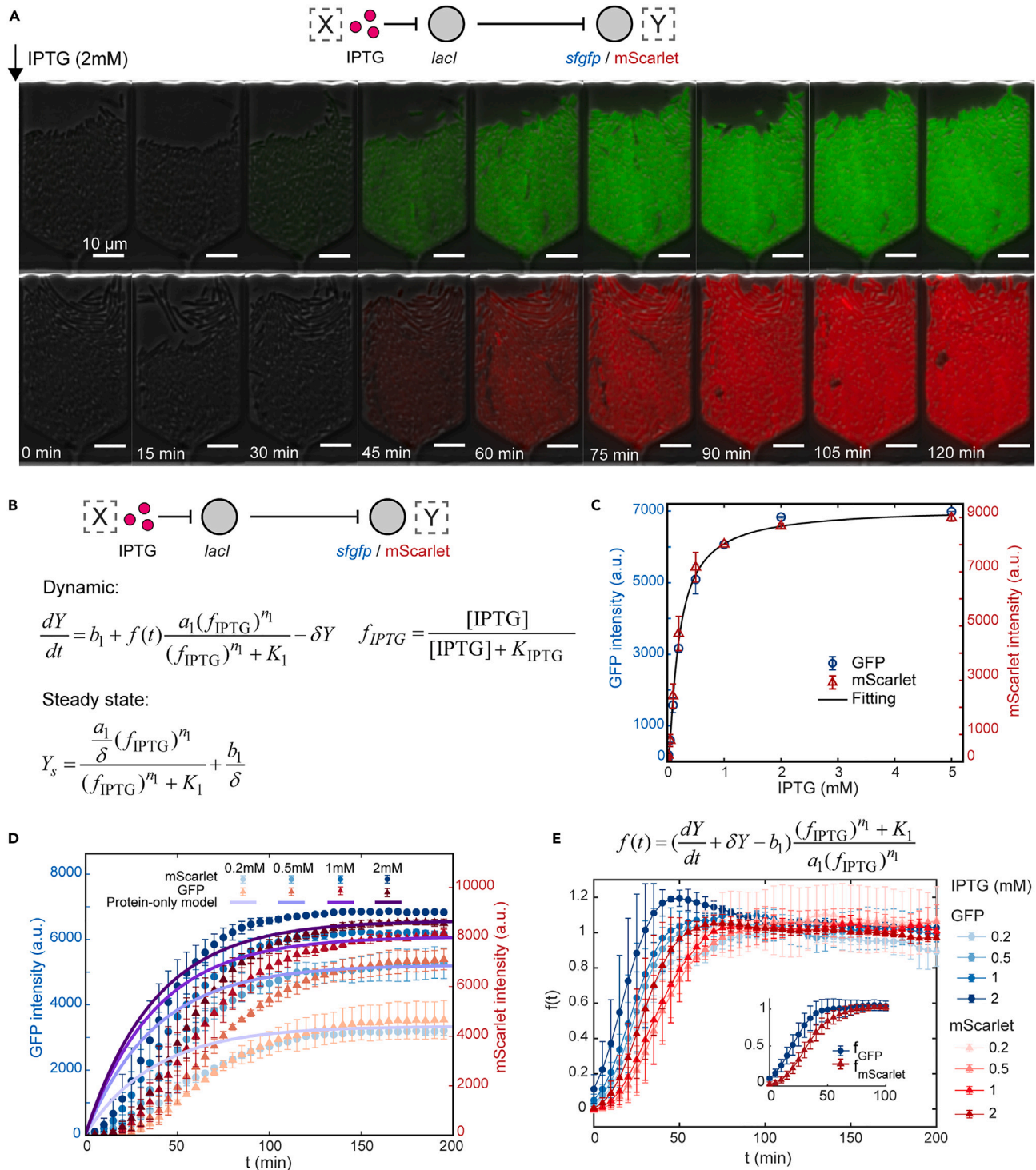
Figure 3. Experimental results of the one-step regulation circuit with sfGFP and mScarlet; sfGFP and mScarlet have different maturation times

(A) Micrograph sequences of monolayer cells expressing sfGFP and mScarlet over time. The expression level of sfGFP increased faster than that of mScarlet. The length of the scale bar is 10 μm.

(B) Mathematic model of one-step regulation.

(C) The steady-state expression levels of sfGFP and mScarlet can be fitted by the same dose-response curve.

(D) Comparison of the dynamic expression levels of sfGFP and mScarlet and the protein-only model simulation results. The data showed that the expression level of sfGFP increased faster than that of mScarlet under the same inducer concentration.

Figure 3. Continued

(E) The equation above the figure shows how to derive $f(t)$ from the experimental data. The experimental $f(t)$ data of sfGFP rose faster than those of mScarlet. The inset shows the average $f(t)$ of all the different inducer concentrations with apparent sfGFP expression. The data are presented as the mean $\pm$ SD (standard deviation) from three experimental repeats. For each experiment, the results of at least 12 trap chamber repeats were averaged.

step function approximation. Since we proved that $f(t) \approx 1$ when $t = T_1$, we set $t = \frac{1}{2}T_1$ as the cut-off point. The approximation function can be written as follows:

$$f_2(t) = \begin{cases} 0 & t < T_2 \\ 1 & t \geq T_2 \end{cases} \qquad T_2 = \left(\frac{1}{\delta+m_Y} + \frac{1}{\delta+d_{m_Y}}\right) \qquad \text{(Equation 12)}$$

A comparison of the simulation results of $f(t)$ and $f_2(t)$ is shown in Figure 2D. When using the step function approximation of $f(t)$ to describe the one-step regulation process, since the input X is continuous and unchangeable, the input was treated as if only takes effect after a time of T_2. The DDM can then be transformed to a DDE-like model as follows:

$$\frac{dY}{dt} = \begin{cases} b - \delta Y & t < T_2 \\ b + a\dfrac{X^n}{X^n+K_X{}^n} - \delta Y & t \geq T_2 \end{cases} \qquad T_2 = \left(\frac{1}{\delta+m_Y} + \frac{1}{\delta+d_{m_Y}}\right) \qquad \text{(Equation 13)}$$

When the input X varied over time as function $X(t)$, $f_2(t)$ type approximation also can be used to simplify the formulas for $\frac{dY}{dt}$ to:

$$\frac{dY}{dt} + \delta Y = b + a\frac{X^n(t - \tau_Y)}{X^n(t - \tau_Y)+K_X{}^n} \qquad \text{(Equation 14)}$$

$$\tau_Y \approx \left(\frac{1}{\delta+m_Y} + \frac{1}{\delta+d_{m_Y}}\right) \qquad \text{(Equation 15)}$$

The delay time τ_Y is the same as the previously derived T_2 (Equation 13) (see STAR Methods for more detail).

Therefore, using step function approximation for every step in the regulation processes, the delay resulting from the transcription-translation processes is approximately $\tau_Y = \left(\frac{1}{\delta+m_Y} + \frac{1}{\delta+d_{m_Y}}\right)$, where d_{m_Y} and m_Y are the mRNA decay rate and the protein maturation rate of the produced protein. Though Equation 14 is similar to other DDE models, the formula of delay time τ_Y from detailed model is solved here which answers the puzzle of delay time used in old DDE models.

The simulations of the expression of protein Y using the protein-only model and the DDM with $f(t)$, $f_1(t)$, and $f_2(t)$ are shown in Figure 2E. The simulation results of the DDM with $f_1(t)$ showed very subtle differences when compared with the simulation results of the DDM using the original $f(t)$ function. The simulation results of the DDM with $f_2(t)$ showed an apparent difference only when t was small; however, for $t > T_2$, the simulation results were very close to the simulation results using the original $f(t)$ function. The simulation results of the protein-only model showed an obvious earlier and faster increase than the simulation results of the DDM (Figure 2E). Both the step function approximation and the linear approximation can be used to predict the gene expression dynamics of synthetic circuits. However, for systems in which downstream nodes are hypersensitive, the linear approximation may be more suitable.

In practice, only T_2 (or τ_Y) need to be determined as the dynamic related parameter. The DDM only have one more parameter (T_2 or τ_Y) than the protein-only model. So, the doses-related steady-state parameters can be determined through the dose-response data, while the dynamic related parameter T_2 can be determined through the dynamic response data.

One-step regulation experiments

As a proof of our theory of the time delay caused by transcription, translation and protein folding/maturation, we constructed two one-step regulation modules in *Escherichia coli* (*E. coli*) with two different fluorescent proteins, sfGFP and mScarlet, which have different maturation times.[34] The fluorescent protein (sfGFP or mScarlet) was controlled by LacI and could be induced by isopropyl β-D-thiogalactopyranoside (IPTG). The micrograph data showed that the circuit with mScarlet had a considerably longer delay time than the circuit with sfGFP (Figure 3A). In addition, these two modules with different fluorescent proteins had the same dose-response curve, which could be described by the same dose-related steady-state parameters (Figures 3B and 3C). The expression of sfGFP increased faster than that of mScarlet (Figure 3D). Moreover, the simulation results of the protein-only model without $f(t)$ increased much faster than the experimental data of either sfGFP or mScarlet (Figure 3D). In other words, there was an obvious time delay that could not be excluded when using the protein-only model to describe dynamic expression levels in synthetic circuits.

After the steady-state parameters were determined, we obtained the $f(t)$s for different concentrations of the inducer IPTG (Figure 3E). For different IPTG concentrations of the same fluorescent protein, the $f(t)$s showed essentially the same trend (Figure 3E). However, compared with mScarlet, the $f(t)$s of sfGFP increased and reached a value of 1 faster, and these results were more obvious after averaging, as shown in the inset of Figure 3E. Based on the experimental data of $f(t)$, we could use the linear approximation function shown in Equation 11 to fit the data and obtain the characteristic time T_1 (Figure 4A). The fitted characteristic time T_1 for sfGFP was approximately 39 min. For mScarlet, the
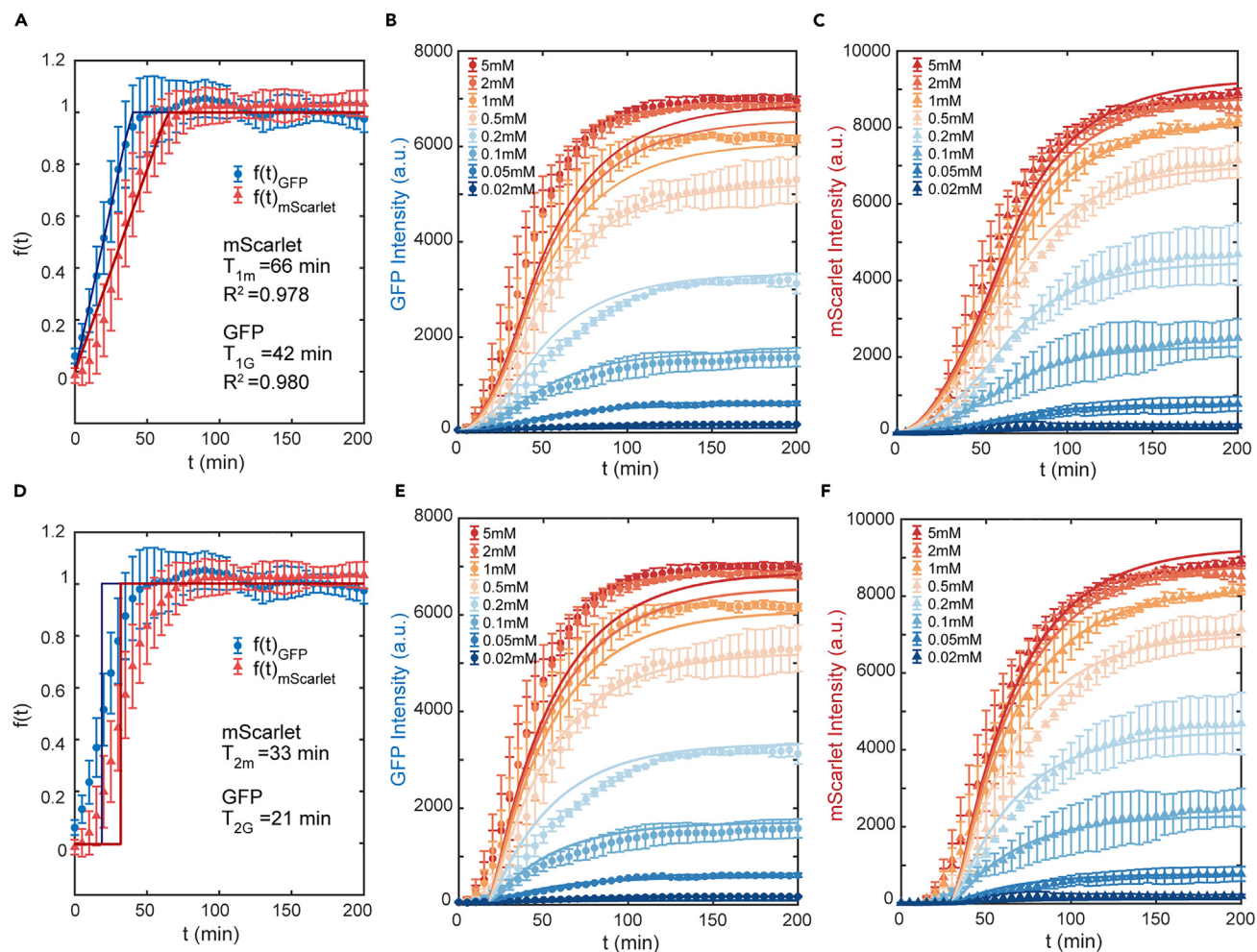
Figure 4. Fitting results of the $f(t)$ s and comparison of the experimental data and the DDM simulation results

(A) Fitting results of the $f(t)$ s using the linear approximation model.

(B and C) Comparison of the sfGFP (B) and mScarlet (C) data and the results of DDM simulations that used the linear approximation model. (D) Experimental $f(t)$ s and the step function approximation model.

(E and F) Comparison of the sfGFP (E) and mScarlet (F) $f(t)$ data and the results of DDM simulations that used the step function approximation. The data are presented as the mean $\pm$ SD (standard deviation) from three experimental repeats. For each experiment, the results of at least 12 trap chamber repeats were averaged.

fitted characteristic time T_1 was approximately 62 min, which was longer than that for sfGFP. However, the fitted characteristic time might be different from the T_1 value calculated with Equation 11. Therefore, we considered reasonable ranges of the two parameters ($m = 0 \sim 1 \text{ min}^{-1}$ and $d_m = 0 \sim 1 \text{ min}^{-1}$, which indicated that the ranges of the half-maturation and half decay times were both $\ln 2 \rightarrow \infty$ min), simulated $f(t)$, and found that the difference $\left(\frac{T_1 - T_{fit}}{T_{fit}}\right)$ between the fitted and the calculated T_1 was less than 10% (Figures S1B and S1C). Furthermore, in most cases, the calculated T_1 was 4~10% larger. Therefore, the fitted characteristic time was comparable to the calculated T_1, and the fitted characteristic delay time was corrected by +7% hereafter. The maturation times of sfGFP and mScarlet in living cells have been studied previously[34]; the half maturation time of sfGFP was determined to be 13.6 ± 0.9 min, the half maturation time of mScarlet was determined to be 25.7 ± 1.5 min,[34] and the half-lives of mRNAs in *E. coli* are mostly between 3 and 8 min,[31] which is considerably shorter than the cell division time. The bacterial growth rate was $\delta = 0.0175 \text{ min}^{-1}$ (Figure S6C). We calculated the corresponding m and d_m for both sfGFP and mScarlet ($m_{GFP} \approx 0.0495 \text{ min}^{-1}$, $m_{mScarlet} \approx 0.0248 \text{ min}^{-1}$, $d_m = 0.087 \sim 0.231 \text{ min}^{-1}$)[31,34] and then calculated T_1. The calculated T_1 for sfGFP should be 38–49 min, and the corrected fitted time was 42 min, which was within the range. The calculated T_1 for mScarlet should be between 55 and 66 min, and the corrected fitted time was 66 min, which was also within the range. This result showed that this method can be used to characterize the time delay caused by transcription-translation processes to some extent.

After T_1 was calculated, the delay function $f_1(t)$ (Equation 11) was determined. Simulations of the DDM (Equation 14) are shown in Figure 4. With $f_1(t)$ added, the simulation results were more consistent with the experimental data (Figures 4B and 4C) than the previous protein-only model

(Figure 3D). The step function approximation could also be derived, with $T_2 = \frac{1}{2}T_1$ (Figure 4D), and simulations of the DDM with $f_2(t)$ (Figures 4E and 4F) also showed much better consistency with the experimental data than the protein-only model (Figure 3D). Although the DDM simulation results did not perfectly match the corresponding experimental data, the model proposed here showed a great improvement over the previous protein-only model. We also built other one-step regulation circuits that can be induced by other chemicals. The outputs of all these circuits were represented by sfGFP. The proteins replacing LacI included NahR, CepR, and RpaR[58] induced by salicylic acid, C4-HSL and pC-HSL respectively. We also calculated $f(t)$s and fitted the characteristic delay times. The results showed that the characteristic delay times were similar to that of the circuit controlled by LacI with sfGFP as the reporter (Figure S2). In other words, the regulatory protein did not affect the characteristic delay time, regardless of the input, and the characteristic delay time was related only to the protein that was being produced.

In conclusion, for one-step regulation processes, the dose-related steady-state determining part and dynamic determining part can be separated in the DDM. Therefore, the doses-related steady-state parameters can be derived based on the dose-response curve, while the dynamic related parameters can be derived based on the dynamic response curves. By combining these two parts, we can obtain a more complete and simpler model to describe the dynamic regulation of synthetic circuits.

Determining all the parameters of the intermediate regulatory protein

Since we previously derived the delay times of sfGFP and mScarlet, corresponding two-step regulation circuits can be built to determine the characteristic delay times and doses-related steady-state parameters of the intermediate proteins. The proposed method is formulated as follows.

As shown in Figure 5A, in a one-step regulation circuit, we used a continuous steady input X to control an output protein Z. First, by fitting the dose-response curve, we obtained the doses-related steady-state parameters. Then, we calculated $f(t)$ based on the experimental data. Next, we fitted $f(t)$ to determine the characteristic delay time τ_Z. Finally, we obtained the dynamic equation of the one-step regulation circuit (Figure 5A). The doses-related steady-state parameters were related to the regulatory property F_1 of X, and the characteristic delay time τ_Z was related to the mRNA decay rate and protein maturation rate of protein Z.

Then, we designed a two-step regulation circuit in which the input X controls Y, and Y controls Z (Figure 5A). The regulatory property F_1 (steady-state Hill-type function with doses-related steady-state parameters: $b_X + a_X \frac{X^n}{X^n + K_X^n}$) of X and the characteristic delay time τ_Z of protein Z have already been determined. Thus, we first fit the experimental dose-response curve to determine the doses-related steady-state parameters which refer to F_2 (steady-state Hill-type function with doses-related steady-state parameters: $b_Y + a_Y \frac{Y^n}{Y^n + K_Y^n}$) of protein Y. And then fit the dynamic response curves to obtain the characteristic delay time τ_Y associated with protein Y (Figure 5A). This method can be used to obtain the regulatory properties and characteristic delay times of various regulatory proteins, and those parameters can be used to construct DDMs to predict the dynamic properties of synthetic circuits.

To determine the parameters of regulatory proteins, including activators and repressors, we built a variety of two-step regulation circuits. These two-step regulation circuits were controlled by LacI or NahR and induced by IPTG or salicylic acid. The activators included T7 RNAPs with four different CI434 binding sites,[28] RpaR, CepR, LuxR[58] and σECF11. RpaR, CepR, and LuxR need specific signal molecules to be activated and show effects, and the corresponding signal molecules were pC-HSL for RpaR and C4-HSL for both CepR and LuxR. The repressors included CI434 with four operators with different binding site designs[28] and λCI. The circuits of the T7 RNAPs and CI434 with different operators were constructed by Zong, Y. et al.[28] The parameters of these regulatory proteins are shown in Table 1. The various regulatory proteins had different characteristic delay times. The activator RpaR had the shortest delay time of 7 min, and the repressor λCI had the longest delay time of 26 min (Table 1). The experimental data and DDM fitting results for the activator LuxR and repressor CI434-O₃ are shown in Figures 5B and 5C, respectively. The experimental data for the other two-step regulation circuits and the corresponding DDM fitting results are shown in Figure S3.

In conclusion, by combining the doses-related regulatory parameters and characteristic delay times obtained by the one-step regulation circuits, two-step regulation circuits could be constructed to inversely determine the doses-related steady-state parameters and the characteristic delay times of intermediate regulatory proteins. Then, the doses-related steady-state parameters and characteristic delay times of the proteins could be used to predict the dynamic responses of synthetic circuits through the DDM. We constructed several synthetic circuits to demonstrate the predictive ability of the DDM.

Dynamic prediction of synthetic circuits

The final goal of mathematic models in synthetic biology applications should be the quantitative prediction of gene expression levels in synthetic circuits. We derived a series of regulatory parameters and characteristic delay times for different regulatory proteins; thus, the next step is testing the reliability and predictive ability of the proposed DDM and the derived characteristic delay times. Here, we built three different types of synthetic circuits based on the previously characterized regulatory proteins. The first type was a cascaded three-step repression circuit (Figure 6A), which was developed to test whether the characteristic delay times derived for the intermediate regulatory proteins and sfGFP were sufficiently reliable to describe the actual time delay of the circuit. The second type was an IFFL circuit with the same node numbers on both the activation and repression sides, which we termed the IFFL type I circuit (Figure 6B). The third type was also an IFFL circuit but with different nodes on the activation and repression sides, which we termed the IFFL type II circuit (Figure 6C). The repression side of the IFFL type II circuit had one more node than the activation side; thus, the repression side should have a much longer delay time than the activation side, which indicated that the dynamic expression of the IFFL type II circuit might show pulsed behavior. In contrast, the IFFL type I circuit had the same number of nodes on both the activation and repression sides; thus, the dynamic expression might not show the obvious pulsed form shown by the IFFL type II circuit.
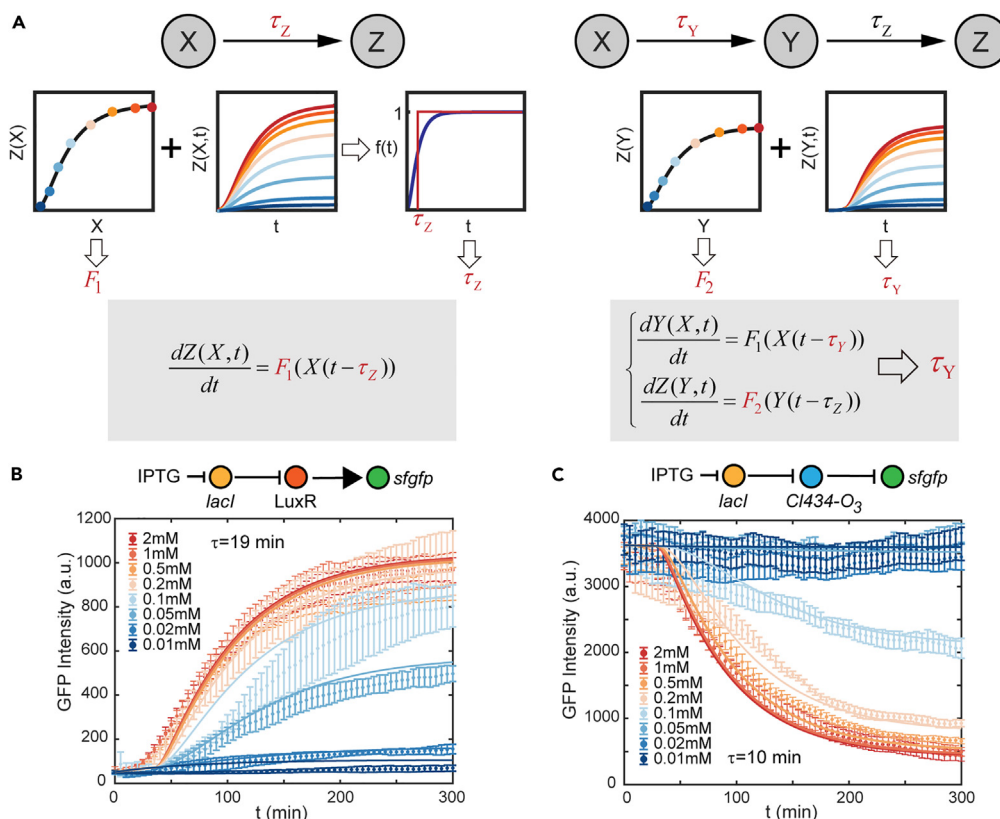
Figure 5. The method to derive the steady-state parameters and the characteristic delay times of intermediate regulatory proteins

(A) By combining the steady-state parameters and the characteristic delay times derived from the one-step regulation circuit, a two-step regulation circuit could be built to derive the parameters of the intermediate proteins.

(B and C) The two-step regulation circuit with IPTG as the input, LuxR (b) and CI434 (c) as the intermediate regulatory proteins, and sfGFP as the output reporter. The dynamic experimental data could be fitted to obtain the characteristic delay times of the LuxR and CI434 proteins. The data are presented as the mean ± SD (standard deviation) from at least 12 trap chamber repeats.

To prove the predictive ability of the DDM, we first constructed four simple cascaded three-step repression circuits (Figure 6A). Each of the circuits was controlled by LacI, which could be induced by IPTG. The second node was the activator T7 RNAP, and the third node was the repressor CI434. There were four operators with different CI434 binding site designs, as constructed by Zong, Y. et al.,[28] resulting in four different repression intensities. The output of all four circuits was sfGFP (Figure 6A). The DDMs of these circuits are shown in STAR Methods. The protein-only model simulation showed an obviously faster decline than the experimental data. However, the DDM simulation results were more consistent with the experimental data (Figures 6A and S4).

The above experiments showed that the DDM could be used to quantitatively predict the dynamic behaviors of simple cascaded circuits. To prove the predictive ability of the DDM for more complicated circuits, we investigated four IFFL type I circuits with different repression operators (Figure 6B), which were constructed by Zong, Y. et al.[28] Each of the four IFFL type I circuits had four nodes: the first node was LacI, which controlled the whole circuit; the second node was T7 RNAP; the third node was CI434; and the output was sfGFP. Four different CI434 operators leaded to four distinct repression intensities. The activator T7 RNAP and the repressor CI434 simultaneously controlled the expression of sfGFP (Figure 6B). As the inhibition strength of the repression operators increased, the IFFL type I circuit showed different dose-response curves[28] (Figure S5A). The activation side and the repression side both had two nodes, which meant that the delay times caused by the two sides should be very similar. Few dynamic changes were observed, and the dynamic modes under different IPTG concentrations mainly simply increased to a plateau (Figure S5B). The DDM of the IFFL type I circuit is shown in STAR Methods. The DDM was first used to predict the dose-response curves of the IFFL type I circuits, and the results showed great quantitative prediction results (Figure S5A). The dose-response curves of the IFFL type I circuits showed that intermediate concentrations of the inducer led to the highest reporter intensity. One dynamic curve of the experimental data of the IFFL type I circuit (O_3, 1 mM IPTG) is shown in Figure 6B. The simulation results of the DDM for different IFFL type I circuits were obviously more consistent with the experimental data than the results of the protein-only model (Figures 6B and S5B).

Although the IFFL type I circuits were more complicated than the previous simple cascaded three-step repression circuits, there were still limited dynamic changes. Most of the dynamics behaviors of these circuits were typical increases (Figure S5B). Therefore, here, we built four

Table 1. Steady state parameters and dynamic related parameters of regulatory elements

Input parameters	Dose-related steady-state parameters						Dynamic related parameter
	a_I	K_{IPTG} (mM)	K_{lac}	n_I	b_I	δ (min^{-1})	τ_{GFP} (min)
LacI	360.68	0.025	1.36	4	0.93	0.0175	21

Input parameters	Dose-related Steady-state parameters					Dynamic related parameter
	a_I	K_I (mM)	n_I	b_I	δ (min^{-1})	τ_{GFP} (min)
Nahr	61.98	0.018	0.73	1.71	0.0175	21
CepR	66.83	0.0639	0.68	17.34	0.0175	21
RpaR	37.17	0.176×10^{-6}	1.45	16.06	0.0175	21

Activators	Dose-related Steady-state parameters					Dynamic related parameter
	a_a	K_a	n_a	b_a	δ (min^{-1})	τ_a (min)
T7 RNAP-O_1	91.68	8.96×10^2	1.39	0.53	0.0175	12
T7 RNAP-O_2	78.74	7.74×10^2	1.40	0.41	0.0175	12
T7 RNAP-O_3	90.56	1.11×10^3	1.28	0.47	0.0175	12
T7 RNAP-O_4	84.56	1.12×10^3	1.20	0.47	0.0175	12
CepR	13.59	2.23×10^2	0.99	1.76	0.0175	22
RpaR	84.64	1.40×10^2	2.04	3.27	0.0175	7
LuxR	18.08	6.32×10^2	1.27	0.90	0.0175	19
σECF11	136.40	8.24×10^2	3.93	5.37	0.0175	13

Repressors	Dose-related Steady-state parameters					Dynamic related parameter
	a_r	K_r	n_r	b_r	δ (min^{-1})	τ_r (min)
CI434-O_1	61.55	3.66×10^3	1.37	0	0.0175	10
CI434-O_2	55.78	7.63×10^2	1.83	10.12	0.0175	10
CI434-O_3	56.67	6.32×10^2	1.95	6.75	0.0175	10
CI434-O_4	58.40	5.04×10^2	2.35	5.99	0.0175	10
λCI	72.27	5.54×10^3	1.74	0	0.0175	26

IFFL type II circuits with different repression operators. The repression sides of all four IFFL type II circuits had one more node than the corresponding activation sides, so the IFFL type II circuits might show pulsed dynamic expression levels over time. The first node was still LacI, which controlled the expression of T7 RNAP, and T7 RNAP controlled both CI434 and sfGFP simultaneously, while CI434 also controlled the expression of sfGFP (Figure 6C). Theoretically, the expression of sfGFP will first increase to a peak; then, the expression is repressed by CI434, and the expression level will decrease to a lower value. The experimental data of the IFFL type II circuit with O_3 under 1 mM IPTG are shown in Figure 6C, which showed that the expression level of sfGFP first increased to a peak and then gradually decreased to a lower value, tending to a steady state. The corresponding simulations of the protein-only model and the DDM are also shown in Figure 6C. The experimental data showed a clear delay compared to the protein-only model simulation, while the DDM perfectly compensated for this delay (Figures 6C and S5C), allowing the DMM to obtain much better quantitative dynamic predictions. The protein-only model simulation results had lower amplitudes than both the experimental data and the DDM simulation results because the times of rising and declining were both shorter when the simulation was performed without the delay times.

Based on all the experiments presented here, we determine that the DDM perfectly combines the delay times caused by transcription-translation processes and the dose-related steady-state parameters, allowing the proposed model to make much better quantitative predictions of the dynamic behaviors in synthetic circuits than the protein-only model. Furthermore, the DDM proposed here make a parameter reduction than the detailed model, which make it easier to determine the dose-related steady-state parameters and the dynamic related parameter through simple experiment. Also, compare with the existing delay models,[55] the DDM proposed here provide a method to derive the parameters of hidden nodes easily from the dose-response curve and the dynamic expression curve separately which make it easier to quantitatively characterize synthetic gene elements with existing data.

DISCUSSION

Researchers in synthetic biology have used bottom-up methods to engineer new regulatory circuits based on simpler components adapted from nature. As the complexity of the circuits increases, it becomes more important to make accurate quantitative predictions based on their constituent parts.[15,59] Hill-type functions have been widely used to quantitatively predict the performance of synthetic circuits.[21,28,29,48] In most cases, the model is simplified without considering the detailed steps in transcription-translation processes because the inclusion of
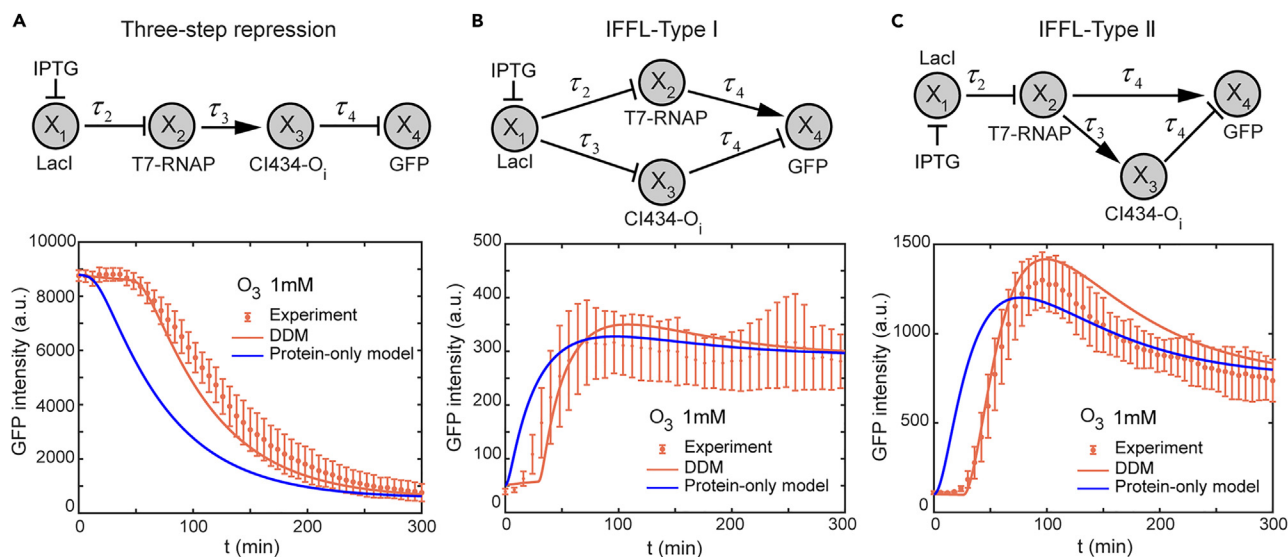
Figure 6. Comparison of the dynamic prediction results between the protein-only model and the DDM

The construction of the cascaded three-step repression circuits (A), IFFL type I circuits (B) and IFFL type II circuits (C) with different operators[28] and the experimental data with the protein-only model and DDM predictions of these circuits (O_3, 1 mM IPTG) are presented. The results show that the DDM obtained much better prediction results than the protein-only model that did not consider delays. The data are presented as the mean ± SD (standard deviation) from at least 12 trap chamber repeats.

more details means that more parameters need to be determined.[47] However, transcription-translation processes may take nonnegligible amounts of time to complete, which may affect the dynamic properties of synthetic circuits.[30,34]

In this work, we started with a one-step regulation circuit based on a detailed ODE model, which used three ODEs to separately describe the transcription, translation to unfolded protein, and protein folding/maturation processes.[39,47] We first proved that the detailed ODE model can be transformed into a DDM, which can be separated into two parts based on a theoretical formulation. One part is related to the dose-related steady state of the circuit, while the other part is related to the dynamic delay caused by the transcription-translation processes. Through simple one-step regulation experiments with different fluorescent proteins, namely, sfGFP and mScarlet, which have different maturation times,[34] we proved that different maturation times led to clear dynamic differences, although the dose-response curves were the same (Figure 3).

After proving the existence of the delay time, which was ignored in the simplified protein-only model, we proposed a method to determine the characteristic delay times of regulatory proteins. We used the DDM to determine the characteristic delay times and dose-related steady-state parameters of intermediate proteins based on a two-step regulation circuit (Figure 5). Then, we used those parameters to predict the dynamic expression levels in more complex synthetic circuits with the DDM. The results suggested that the DDM could perfectly compensate for the delay times caused by transcription-translation processes and obtain much better quantitative predictions of the dynamic expression levels in synthetic circuits than previous protein-only model. The synthetic gene circuits studied here were relatively simple, however, the method of using DDM to quantitatively characterize synthetic gene units was proved useful. The effects of the delay error may be more significant for larger cascading networks. And theoretical studies of delays showed that increasing delay could dramatically increase the mean residence times near stable states of bistable circuits.[48] The synthetic circuits constructed here were all relatively simple feedforward circuits, but the method proposed here were theoretically universal, which can easily be applied to character synthetic gene units and predict dynamic expression levels in various complex circuits. Circuits with feedback regulations can also be built in the future for further study of the effects of delays on complicated gene circuits.

Limitations of the study

The synthetic gene circuits studied here were relatively simple, and all feedforward circuits, though the method of using DDM to quantitatively characterize synthetic gene units were proved useful. The effects of the delay error may be more significant for larger cascading networks. More complicated circuits with feedback regulations may need to be built in the future for further study of the effects of delays on complicated gene expression dynamics.

STAR★METHODS

Detailed methods are provided in the online version of this paper and include the following:

- KEY RESOURCES TABLE
- RESOURCE AVAILABILITY
  - Lead contact

SUPPLEMENTAL INFORMATION

Supplemental information can be found online at https://doi.org/10.1016/j.isci.2024.109142.

AUTHOR CONTRIBUTIONS

Conceptualization: C.L., F.Z., and Y.S. Methodology: C.L., F.Z., and Y.S. Investigation: C.L., F.Z., and Y.S. Visualization: C.L., Y.S., and Q.O. Supervision: C.L, Writing—original draft: C.L., Y.S., and F.Z. Writing—review and editing: C.L., Y.S., F.Z., and Q.O.

DECLARATION OF INTERESTS

The authors declare no competing interests.

REFERENCES

1. Yosef, N., and Regev, A. (2011). Impulse control: temporal dynamics in gene transcription. Cell *144*, 886–896. https://doi.org/10.1016/j.cell.2011.02.015.

2. Shen-Orr, S.S., Milo, R., Mangan, S., and Alon, U. (2002). Network motifs in the transcriptional regulation network of Escherichia coli. Nat. Genet. *31*, 64–68. https://doi.org/10.1038/ng881.

3. Ma, W., Trusina, A., El-Samad, H., Lim, W.A., and Tang, C. (2009). Defining network topologies that can achieve biochemical adaptation. Cell *138*, 760–773. https://doi.org/10.1016/j.cell.2009.06.013.

4. Lagage, V., and Uphoff, S. (2020). Pulses and delays, anticipation and memory: seeing bacterial stress responses from a single-cell perspective. FEMS Microbiol. Rev. *44*, 565–571. https://doi.org/10.1093/femsre/fuaa022.

5. Mitchell, A., Romano, G.H., Groisman, B., Yona, A., Dekel, E., Kupiec, M., Dahan, O., and Pilpel, Y. (2009). Adaptive prediction of environmental changes by microorganisms. Nature *460*, 220–224. https://doi.org/10.1038/nature08112.

6. Karin, O., Swisa, A., Glaser, B., Dor, Y., and Alon, U. (2016). Dynamical compensation in physiological circuits. Mol. Syst. Biol. *12*, 886. https://doi.org/10.15252/msb.20167216.

7. Levine, J.H., Lin, Y., and Elowitz, M.B. (2013). Functional Roles of Pulsing in Genetic Circuits. Science *342*, 1193–1200. https://doi.org/10.1126/science.1239999.

8. Bashor, C.J., and Collins, J.J. (2018). Understanding Biological Regulation Through Synthetic Biology. Annu. Rev. Biophys. *47*, 399–423. https://doi.org/10.1146/annurev-biophys-070816-033903.

9. Basu, S., Mehreja, R., Thiberge, S., Chen, M.-T., and Weiss, R. (2004). Spatiotemporal control of gene expression with pulse-generating networks. Proc. Natl. Acad. Sci. USA *101*, 6355–6360. https://doi.org/10.1073/pnas.0307571101.

10. Flores Bueso, Y., and Tangney, M. (2017). Synthetic Biology in the Driving Seat of the Bioeconomy. Trends Biotechnol. *35*, 373–378. https://doi.org/10.1016/j.tibtech.2017.02.002.

11. Wan, X., Volpetti, F., Petrova, E., French, C., Maerkl, S.J., and Wang, B. (2019). Cascaded amplifying circuits enable ultrasensitive cellular sensors for toxic metals. Nat. Chem. Biol. *15*, 540–548. https://doi.org/10.1038/s41589-019-0244-3.

12. Kim, H.J., Jeong, H., and Lee, S.J. (2018). Synthetic biology for microbial heavy metal biosensors. Anal. Bioanal. Chem. *410*, 1191–1203. https://doi.org/10.1007/s00216-017-0751-6.

13. Zhang, F., Car, J.M., and Keasling, J.D. (2012). Design of a dynamic sensor-regulator system for production of chemicals and fuels derived from fatty acids. Nat. Biotechnol. *30*, 354–359. https://doi.org/10.1038/nbt.2149.

14. Cameron, D.E., Bashor, C.J., and Collins, J.J. (2014). A brief history of synthetic biology. Nat. Rev. Microbiol. *12*, 381–390. https://doi.org/10.1038/nrmicro3239.

15. Purnick, P.E.M., and Weiss, R. (2009). The second wave of synthetic biology: from modules to systems. Nat. Rev. Mol. Cell Biol. *10*, 410–422. https://doi.org/10.1038/nrm2698.

16. Zhang, C., Tsoi, R., and You, L. (2016). Addressing biological uncertainties in engineering gene circuits. Integr. Biol. *8*, 456–464. https://doi.org/10.1039/c5ib00275c.

17. Lopatkin, A.J., and Collins, J.J. (2020). Predictive biology: modelling, understanding and harnessing microbial complexity. Nat.

Rev. Microbiol. *18*, 507–520. https://doi.org/10.1038/s41579-020-0372-5.

18. Ryan, J., Hong, S., Foo, M., Kim, J., and Tang, X. (2022). Model-Based Investigation of the Relationship between Regulation Level and Pulse Property of I1-FFL Gene Circuits. ACS Synth. Biol. *11*, 2417–2428. https://doi.org/10.1021/acssynbio.2c00109.

19. Car, J.M., Goler, J.A., Juminaga, D., and Keasling, J.D. (2011). Model-Driven Engineering of RNA Devices to Quantitatively Program Gene Expression. Science *334*, 1716–1719. https://doi.org/10.1126/science.1212209.

20. O'Brien, E.L., Itallie, E.V., and Bennett, M.R. (2012). Modeling synthetic gene oscillators. Math. Biosci. *236*, 1–15. https://doi.org/10.1016/j.mbs.2012.01.001.

21. Ellis, T., Wang, X., and Collins, J.J. (2009). Diversity-based, model-guided construction of synthetic gene networks with predicted functions. Nat. Biotechnol. *27*, 465–471. https://doi.org/10.1038/nbt.1536.

22. Gardner, T.S., Cantor, C.R., and Collins, J.J. (2000). Construction of a genetic toggle switch in Escherichia coli. Nature *403*, 339–342. https://doi.org/10.1038/35002131.

23. Elowitz, M.B., and Leibler, S. (2000). A synthetic oscillatory network of transcriptional regulators. Nature *403*, 335–338. https://doi.org/10.1038/35002125.

24. Shi, W., Ma, W., Xiong, L., Zhang, M., and Tang, C. (2017). Adaptation with transcriptional regulation. Sci. Rep. *7*, 42648. https://doi.org/10.1038/srep42648.

25. Zhang, F., Sun, Y., Zhang, Y., Shen, W., Wang, S., Ouyang, Q., and Luo, C. (2022). Independent control of amplitude and period in a synthetic oscillator circuit with modified repressilator. Commun. Biol. *5*, 23. https://doi.org/10.1038/s42003-021-02987-1.

26. Krishnanathan, K., Anderson, S.R., Billings, S.A., and Kadirkamanathan, V. (2012). A Data-Driven Framework for Identifying Nonlinear Dynamic Models of Genetic Parts. ACS Synth. Biol. *1*, 375–384. https://doi.org/10.1021/sb300009t.

27. Davidsohn, N., Beal, J., Kiani, S., Adler, A., Yaman, F., Li, Y., Xie, Z., and Weiss, R. (2015). Accurate predictions of genetic circuit behavior from part characterization and modular composition. ACS Synth. Biol. *4*, 673–681. https://doi.org/10.1021/sb500263b.

28. Zong, Y., Zhang, H.M., Lyu, C., Ji, X., Hou, J., Guo, X., Ouyang, Q., and Lou, C. (2017). Insulated transcriptional elements enable precise design of genetic circuits. Nat. Commun. *8*, 52. https://doi.org/10.1038/s41467-017-00063-z.

29. Rosenfeld, N., Young, J.W., Alon, U., Swain, P.S., and Elowitz, M.B. (2007). Accurate prediction of gene feedback circuit behavior from component properties. Mol. Syst. Biol. *3*, 143. https://doi.org/10.1038/msb4100185.

30. Proshkin, S., Rahmouni, A.R., Mironov, A., and Nudler, E. (2010). Cooperation between translating ribosomes and RNA polymerase in transcription elongation. Science *328*, 504–508. https://doi.org/10.1126/science.1184939.

31. Bernstein, J.A., Khodursky, A.B., Lin, P.-H., Lin-Chao, S., and Cohen, S.N. (2002). Global analysis of mRNA decay and abundance in *Escherichia coli* at single-gene resolution using two-color fluorescent DNA microarrays.

Proc. Natl. Acad. Sci. USA *99*, 9697–9702. https://doi.org/10.1073/pnas.0308747101.

32. Wang, Y., Liu, C.L., Storey, J.D., Tibshirani, R.J., Herschlag, D., and Brown, P.O. (2002). Precision and functional specificity in mRNA decay. Proc. Natl. Acad. Sci. USA *99*, 5860–5865. https://doi.org/10.1073/pnas.092538799.

33. Schwanhäusser, B., Busse, D., Li, N., Dittmar, G., Schuchhardt, J., Wolf, J., Chen, W., and Selbach, M. (2011). Global quantification of mammalian gene expression control. Nature *473*, 337–342. https://doi.org/10.1038/nature10098.

34. Balleza, E., Kim, J.M., and Cluzel, P. (2018). Systematic characterization of maturation time of fluorescent proteins in living cells. Nat. Methods *15*, 47–51. https://doi.org/10.1038/nmeth.4509.

35. Finkelstein, A.V., Bogatyreva, N.S., Ivankov, D.N., and Garbuzynskiy, S.O. (2022). Protein folding problem: enigma, paradox, solution. Biophys. Rev. *14*, 1255–1272. https://doi.org/10.1007/s12551-022-01000-1.

36. Ivankov, D.N., Garbuzynskiy, S.O., Alm, E., Plaxco, K.W., Baker, D., and Finkelstein, A.V. (2003). Contact order revisited: Influence of protein size on the folding rate. Protein Sci. *12*, 2057–2062. https://doi.org/10.1110/ps.0302503.

37. Potvin-Trottier, L., Lord, N.D., Vinnicombe, G., and Paulsson, J. (2016). Synchronous long-term oscillations in a synthetic gene circuit. Nature *538*, 514–517. https://doi.org/10.1038/nature19841.

38. Luro, S., Potvin-Trottier, L., Okumus, B., and Paulsson, J. (2020). Isolating live cells after high-throughput, long-term, time-lapse microscopy. Nat. Methods *17*, 93–100. https://doi.org/10.1038/s41592-019-0620-7.

39. Stricker, J., Cookson, S., Bennett, M.R., Mather, W.H., Tsimring, L.S., and Hasty, J. (2008). A fast, robust and tunable synthetic gene oscillator. Nature *456*, 516–519. https://doi.org/10.1038/nature07389.

40. Panda, S. (2016). Circadian physiology of metabolism. Science *354*, 1008–1015. https://doi.org/10.1126/science.aah4967.

41. Scheiermann, C., Gibbs, J., Ince, L., and Loudon, A. (2018). Clocking in to immunity. Nat. Rev. Immunol. *18*, 423–437. https://doi.org/10.1038/s41577-018-0008-4.

42. Webb, A.A.R., Seki, M., Satake, A., and Caldana, C. (2019). Continuous dynamic adjustment of the plant circadian oscillator. Nat. Commun. *10*, 550. https://doi.org/10.1038/s41467-019-08398-5.

43. Tomazou, M., Barahona, M., Polizzi, K.M., and Stan, G.B. (2018). Computational Re-design of Synthetic Genetic Oscillators for Independent Amplitude and Frequency Modulation. Cell Syst. *6*, 508–520.e5. https://doi.org/10.1016/j.cels.2018.03.013.

44. Westbrook, A., Tang, X., Marshall, R., Maxwell, C.S., Chappell, J., Agrawal, D.K., Dunlop, M.J., Noireaux, V., Beisel, C.L., Lucks, J., and Franco, E. (2019). Distinct timescales of RNA regulators enable the construction of a genetic pulse generator. Biotechnol. Bioeng. *116*, 1139–1151. https://doi.org/10.1002/bit.26918.

45. Megerle, J.A., Fritz, G., Gerland, U., Jung, K., and Rädler, J.O. (2008). Timing and dynamics of single cell gene expression in the arabinose utilization system. Biophys. J. *95*,

2103–2115. https://doi.org/10.1529/biophysj.107.127191.

46. Roussel, M.R. (1996). The Use of Delay Differential Equations in Chemical Kinetics. J. Phys. Chem. *100*, 8323–8330. https://doi.org/10.1021/jp9600672.

47. Rosenfeld, N., and Alon, U. (2003). Response delays and the structure of transcription networks. J. Mol. Biol. *329*, 645–654. https://doi.org/10.1016/s0022-2836(03)00506-0.

48. Gupta, C., López, J.M., Ott, W., Josić, K., and Bennett, M.R. (2013). Transcriptional Delay Stabilizes Bistable Gene Networks. Phys. Rev. Lett. *111*, 058104. https://doi.org/10.1103/physrevlett.111.058104.

49. Feng, J., Sevier, S.A., Huang, B., Jia, D., and Levine, H. (2016). Modeling delayed processes in biological systems. Phys. Rev. E *94*, 032408. https://doi.org/10.1103/physreve.94.032408.

50. Glass, D.S., Jin, X., and Riedel-Kruse, I.H. (2021). Nonlinear delay differential equations and their application to modeling biological network motifs. Nat. Commun. *12*, 1788. https://doi.org/10.1038/s41467-021-21700-8.

51. Tang, H. (2022). Uncertain chemical reaction equation with delay. J. Ambient Intell. Hum. Comput. *14*, 3867–3874. https://doi.org/10.1007/s12652-022-04458-9.

52. Bratsun, D., Volfson, D., Tsimring, L.S., and Hasty, J. (2005). Delay-induced stochastic oscillations in gene regulation. Proc. Natl. Acad. Sci. USA *102*, 14593–14598. https://doi.org/10.1073/pnas.0503858102.

53. Mahaffy, J.M., and Pao, C.V. (1984). Models of genetic control by repression with time delays and spatial effects. J. Math. Biol. *20*, 39–57. https://doi.org/10.1007/BF00275860.

54. Mahaffy, J.M. (1984). Cellular control models with linked positive and negative feedback and delays. I. The models. J. Theor. Biol. *106*, 89–102. https://doi.org/10.1016/0022-5193(84)90011-0.

55. Yildirim, N., and Mackey, M.C. (2003). Feedback regulation in the lactose operon: a mathematical modeling study and comparison with experimental data. Biophys. J. *84*, 2841–2851. https://doi.org/10.1016/S0006-3495(03)70013-7.

56. Gedeon, T., Humphries, A.R., Mackey, M.C., Walther, H.-O., and Wang, Z. (2021). Operon dynamics with state dependent transcription and/or translation delays. J. Math. Biol. *84*, 2. https://doi.org/10.1007/s00285-021-01693-0.

57. Sun, Y., Zhang, F., Li, L., Chen, K., Wang, S., Ouyang, Q., and Luo, C. (2022). Two-Layered Microfluidic Devices for High-Throughput Dynamic Analysis of Synthetic Gene Circuits in E. coli. ACS Synth. Biol. *11*, 3954–3965. https://doi.org/10.1021/acssynbio.2c00307.

58. Du, P., Zhao, H., Zhang, H., Wang, R., Huang, J., Tian, Y., Luo, X., Luo, X., Wang, M., Xiang, Y., et al. (2020). De novo design of an intercellular signaling toolbox for multi-channel cell–cell communication and biological computation. Nat. Commun. *11*, 4226. https://doi.org/10.1038/s41467-020-17993-w.

59. Lucks, J.B., Qi, L., Whitaker, W.R., and Arkin, A.P. (2008). Toward scalable parts families for predictable design of biological circuits. Curr. Opin. Microbiol. *11*, 567–573. https://doi.org/10.1016/j.mib.2008.10.002.

STAR★METHODS

KEY RESOURCES TABLE

REAGENT or RESOURCE	SOURCE	IDENTIFIER
Bacterial and virus strains		
E. coli Top10	yuanye	S32803-100ul
E. coli DHL807	Potvin's work[37]	N/A
Chemicals, peptides, and recombinant proteins		
Yeast extract	Oxoid	lp0021
Tryptone	Oxoid	LP0042B
Sodium chloride	tgchem	112008
Agar	Sigma-Aldrich	A1296-500G
IPTG	GPC	AC367-5G
Salicylic acid	Anneji	W610518
N-butyryl-L-Homoserine lactone (C4-HSL)	APExBIO	C5727-10
N-(*p*-Coumaroyl)-L-homoserine lactone (pC-HSL)	Santa cruz	sc-301256
Chloramphenicol	abcom	C8050-10
Ampicillin sodium	GPC	AK052-25g
Software and algorithms		
MATLAB 2021	N/A	https://www.mathworks.com/
ImageJ	N/A	https://imagej.nih.gov/ij/
NIS-Elements AR	NIKON	https://www.microscope.healthcare.nikon.com/
Simulation Codes	MATLAB2021	https://github.com/YanhonSun/Code-SI

RESOURCE AVAILABILITY

Lead contact

Further information and requests for resources and reagents should be directed to and will be fulfilled by the lead contact, Chunxiong Luo (pkuluocx@pku.edu.cn).

Materials availability

This study did not generate new unique reagents.

Data and code availability

- Data reported in this paper will be shared by the lead contact upon request.
- All the simulation codes are provided at https://github.com/YanhonSun/Code-SI and publicly available as of the date of publication.
- Any additional information required to reanalyze the data reported in this paper is available from the lead contact upon request.

EXPERIMENTAL MODEL AND STUDY PARTICIPANT DETAILS

Strains

	Plasmid1 (Cmr-pSC101*)	Plasmid2 (Ampr-P15A*)	Source
One-step regulation	–	LacI-GFP	This work. See supplemental information for more detail
	–	LacI-mScarlet	This work. See supplemental information for more detail
	–	RpaR-GFP	This work. See supplemental information for more detail
	–	CepR-GFP	This work. See supplemental information for more detail
	–	NahR-GFP	This work. See supplemental information for more detail

(Continued on next page)

Continued

	Plasmid1 (Cmr-pSC101*)	Plasmid2 (Ampr-P15A*)	Source
Two-step regulation	P$_{Rpa}$-GFP	LacI-RpaR	This work. See supplemental information for more detail
	P$_{Cep}$-GFP	LacI-CepR	This work. See supplemental information for more detail
	P$_{Lux}$-GFP	LacI-LuxR	This work. See supplemental information for more detail
	P$_{\lambda CI}$-GFP	LacI-λCI	This work. See supplemental information for more detail
	P$_{\sigma ECF11}$-GFP	NahR-σECF11	This work. See supplemental information for more detail
	P$_{T7\ RNAP\ (Oi)}$-GFP	LacI (P$_{TAC}$-T7 RNAP in Chromosome)	Yeqing Zong's work: https://doi.org/10.1038/s41467-017-00063-z
	P$_{CI434\ (Oi)}$-GFP	LacI-CI434	Yeqing Zong's work
Three-step repression	P$_{CI434\ (Oi)}$-GFP	LacI (P$_{TAC}$-T7 RNAP in Chromosome) P$_{T7\ RNAP}$-CI434	Yeqing Zong's work
IFFL-Type I	P$_{T7\ RNAP+CI434\ (Oi)}$-GFP	LacI (P$_{TAC}$-T7 RNAP in Chromosome) P$_{TAC}$-CI434	This work. See supplemental information for more detail
IFFL-Type II	P$_{T7\ RNAP+CI434\ (Oi)}$-GFP	LacI (P$_{TAC}$-T7 RNAP in Chromosome) P$_{T7\ RNAP}$-CI434	This work. See supplemental information for more detail

E. coli Top10 was used for plasmid construction, and *E. coli* DHL807 from Potvin's work[37] was used for circuit measuring throughout this study.
*Plasmids without functional elements were obtained from Yeqing Zong's work.[28]

METHOD DETAILS

Strains and plasmids

The plasmids used for the IFFL type I circuits and two-step regulation circuits for T7 RNAP and CI434 were obtained from Zong, Y. et al.[28] The activators CepR, RpaR and LuxR were obtained from Du, P. et al.[58] The sequences of the gene elements and plasmids are shown in Tables S1, S2, and S3. The bacteria were cultured in LB medium, which consisted of 10 g/L tryptone, 5 g/L yeast extract, and 10 g/L NaCl. To make the agar plates, 15 g/L agar was added. The bacteria were cultured at a temperature of 37°C. The antibiotics used here were ampicillin at a final concentration of 100 μg/L derived from a 100 mg/mL aqueous stock and chloramphenicol at a final concentration of 34 μg/mL derived from a 34 mg/mL stock dissolved in ethanol. The inducer isopropyl-β-D-1-thiogalactopyranoside (IPTG) was prepared at different concentrations for various experiments from a 1 M aqueous stock. The autoinducer N-butyryl-homoserine lactone (C4-HSL) was stocked in ethanol at a concentration of 10 mM. The autoinducer *p*-coumaroyl-HSL (pC) was stocked in DMSO at a concentration of 10 mM. For the one-step regulation circuits (RpaR-GFP and CepR-GFP), the signal molecules were added at eight different concentrations (Figure S2). For the two-step regulation circuits (LacI-RpaR-GFP, LacI-CepR-GFP and LacI-LuxR-GFP), the signal molecule concentrations were set to saturation conditions: 100 nM pC-HSL for RpaR and 10 μM C4-HSL for both CepR and LuxR.

Live-cell imaging and data acquisition

We used a high-throughput two-layer PDMS microfluidic chip[57] for live-cell imaging to determine the dynamic gene expression level in synthetic gene circuits under eight inducer concentrations. The detailed design of the microfluidic chip is shown in Figure S6A. A vacuum treatment (15–20 min) was applied to evacuate the air in the PDMS chip to successfully load the bacteria into the chambers without generating any bubbles in the trap area. A microvalve was used to prevent cross contamination in the chip. Before loading the bacteria, the microvalve was closed using a general mechanical pump to push a 1-mL syringe full of water connected by a flexible tube at a speed of 50 μL/min for ~25 s[57] (Figure S6B). A 5-mL syringe containing normal medium without any inducers was connected to another one-pass-eight chip, which was connected to the two-layer chip for 2 h of normal cell culture before the induction of the synthetic circuits, and eight 1-mL syringes containing media with different concentrations of inducers were connected to the corresponding chip inlets (Figure S6B). The microvalve was opened when injecting the normal culture medium and the medium with the inducer added. The chip was placed on a Nikon Ti-E inverted fluorescence microscope for time-lapse imaging with a plan Apo 60× oil immersion objective. The temperature of the incubator system was set to 37°C. The images were captured with an EMCCD camera (Andor DU897). The flow rate of the medium was 40 μL/h, and the images were captured every 5 min for 8 h or longer.

ImageJ software was used to derive data from the experimental microscopic images. An irregular circle was delineated to track an area full of cells, with abnormal cells excluded.[57] The mean fluorescence intensity of the circled area was derived. We used the batch measurement function to derive the time series of the fluorescence intensity. The background was removed by subtracting the mean fluorescence intensity of the area containing no cells. The data from every experiment with different synthetic circuits were derived by averaging the mean fluorescence intensity for at least 12 trap chambers. The growth rate was determined by exponential fitting of the change in the bacterial growth area under conditions with and without the inducer. The growth rate with the inducer was similar to the growth rate without the inducer.[57] We derived the growth rates under different conditions and averaged the values to determine a growth rate of 0.0175 min^{-1} (Figure S6C).

Data analysis and modeling

The steady-state parameters were obtained by fitting the dose-response curve using the "lsqcurvefit" function in MATLAB (version R2021b). Numerical simulations were performed in MATLAB using the "ode45" function for the protein-only model and the "ddesd" function for all the DDMs, including the DDMs for the two-step regulation circuits, three-step regulation circuits, IFFL type I circuits and IFFL type II circuits. The characteristic delay times of the intermediate regulatory proteins were obtained by considering a range of possible values, performing the corresponding simulations for all inducer concentrations, and then selecting the value with the greatest R^2. All the simulation codes are provided at https://github.com/YanhonSun/Code-SI.

Model

One-step regulation model

Here, we present a detailed derivation for the DDM of the one-step regulation circuit. We start with the detailed ODE model, which includes transcription, translation and protein folding/maturation:

$$\frac{dR_Y}{dt} = b' + a'\frac{X^n}{X^n+K_X{}^n} - (\delta + d_m)R_Y$$

$$\frac{dU}{dt} = kR_Y - \delta U - mU \qquad \text{(Equation 16)}$$

$$\frac{dY}{dt} = mU - \delta Y$$

where R_Y is the mRNA concentration, b' and a' are the basal and maximal transcription rates, K_X is the dissociation constant, n is the Hill coefficient, and d_m is the mRNA decay rate. Here, U is the unfolded protein, and Y is the folded (e.g., regulatory) or matured (e.g., fluorescent) protein, k is the translation rate, and m is the protein folding/maturation rate, and δ is the dilution rate due to cell division.

When t = 0, which refers to the steady state before adding X,

$$Y = \frac{mkb'}{\delta(\delta+d_m)(\delta+m)} \qquad \text{(Equation 17)}$$

When t → ∞, which refers to the steady state after the onset of gene regulation with the effect of X,

$$Y = \frac{mk}{\delta(\delta+d_m)(\delta+m)}\left(b' + a'\frac{X^n}{X^n+K_X{}^n}\right) \qquad \text{(Equation 18)}$$

This detailed ODE model could be transformed into a third-order ODE as follows:

$$\frac{d^3Y}{dt^3} = mkb' + mka'\frac{X^n}{X^n+K_X{}^n} - (3\delta + d_m + m)\frac{d^2Y}{dt^2} - (3\delta^2 + 2\delta m + 2\delta d_m + md_m)\frac{dY}{dt} - \delta(\delta + m)(\delta + d_m)Y \qquad \text{(Equation 19)}$$

The eigenvalues are as follows:

$$\lambda_1 = -\delta, \lambda_2 = -(\delta + m), \lambda_3 = -(\delta + d_m) \qquad \text{(Equation 20)}$$

Then, we can derive the function of $Y(t)$ as follows:

$$Y(t) = \sum_{i=1}^{3} C_i e^{\lambda_i t} + \frac{1}{\delta m d_m}(1 - e^{-\delta t})\left[mkb' + mka'\frac{X^n}{X^n+K_X{}^n}\right] - \frac{1}{m(d_m - m)}\frac{1}{\delta+m}(1 - e^{-(\delta+m)t})\left[mkb' + mka'\frac{X^n}{X^n+K_X{}^n}\right]$$

$$+ \frac{1}{d_m(d_m - m)}\frac{1}{\delta+d_m}(1 - e^{-(\delta+d_m)t})\left[mkb' + mka'\frac{X^n}{X^n+K_X{}^n}\right]$$

$$\text{(Equation 21)}$$

The detailed ODE model should have the same steady state as the protein-only model:

$$\frac{dY}{dt} = b + a\frac{X^n}{X^n+K_X{}^n} - \delta Y$$

$$t = 0, Y = \frac{b}{\delta}; \qquad \text{(Equation 22)}$$

$$t \to \infty, Y = \frac{b}{\delta} + \frac{a}{\delta}\frac{X^n}{X^n+K_X{}^n}$$

Therefore, we obtain:

$$a = \frac{mka'}{(\delta+m)(\delta+d_m)}, b = \frac{mkb'}{(\delta+m)(\delta+d_m)}$$

(Equation 23)

Then, we can derive the following equation:

$$\frac{dY}{dt} + \delta Y = -\left(mC_2 e^{-(\delta+m)t} + d_m C_3 e^{-(\delta+d_m)t}\right)$$
$$+ \left[1 + \frac{(\delta+m)e^{-(\delta+d_m)t} - (\delta+d_m)e^{-(\delta+m)t}}{d_m - m}\right]\left[b + a\frac{X^n}{X^n+K_X^n}\right]$$

(Equation 24)

The unknown parameters can be derived through the boundary conditions as follows:

$$t = 0, \quad \begin{cases} Y = C_1 + C_2 + C_3 = \dfrac{b}{\delta} \\[2mm] \dfrac{dY}{dt} + \delta Y = -(mC_2 + d_m C_3) = b \\[2mm] \dfrac{d^2Y}{dt^2} = C_1\delta^2 + C_2(\delta+m)^2 + C_3(\delta+d_m)^2 = 0 \end{cases}$$

(Equation 25)

$$C_1 = \frac{b}{\delta} - (C_2 + C_3), \quad C_2 = \frac{-(\delta+d_m)b}{m(d_m - m)}, \quad C_3 = \frac{(\delta+m)b}{d_m(d_m - m)}$$

(Equation 26)

Finally, we can obtain the DDM as follows:

$$\frac{dY}{dt} + \delta Y = b + \left[1 + \frac{(\delta+m)e^{-(\delta+d_m)t} - (\delta+d_m)e^{-(\delta+m)t}}{d_m - m}\right]\left[a\frac{X^n}{X^n+K_X^n}\right]$$

(Equation 27)

Approximation of $f(t)$

The delay function is formulated as follows:

$$f(t) = 1 + \frac{(\delta+m)e^{-(\delta+d_m)t} - (\delta+d_m)e^{-(\delta+m)t}}{d_m - m}$$

(Equation 28)

where d_m is the mRNA decay rate, m is the protein folding/maturation rate, and δ is the growth rate.

Generally, protein maturation may require more time than mRNA decay. Furthermore, bacterial division may require more time than protein maturation. Therefore, we assumed that $d_m > m > \delta$. When $t = 2\left(\frac{1}{\delta+m} + \frac{1}{\delta+d_m}\right)$, $x = \frac{\delta+d_m}{\delta+m} > 1$, and we have

$$f(t) = 1 + \frac{e^{-2}}{d_m - m}\left[(\delta+m)e^{\frac{-2(\delta+d_m)}{\delta+m}} - (\delta+d_m)e^{\frac{-2(\delta+m)}{\delta+d_m}}\right]$$
$$= 1 + \frac{e^{-2}(\delta+d_m)}{d_m - m}\left(\frac{1}{x}e^{-2x} - e^{-\frac{2}{x}}\right)$$
$$= 1 - \frac{e^{-2\left(1+\frac{1}{x}\right)}(\delta+d_m)}{d_m - m} + \frac{e^{-2(1+x)}(\delta+d_m)}{x(d_m - m)}$$
$$= 1 - \frac{x}{x-1}e^{-2\left(1+\frac{1}{x}\right)} + \frac{e^{-2(1+x)}}{x-1} \geq 1 - e^{-2}$$

(Equation 29)

This result indicates that when $t = 2\left(\frac{1}{\delta+m} + \frac{1}{\delta+d_m}\right)$, the $f(t)$ value is very close to 1. Therefore, we proposed the following linear approximation:

$$f_1(t) = \begin{cases} \dfrac{t}{T_1} & t < T_1 \\[2mm] 1 & t \geq T_1 \end{cases} \quad T_1 = 2\left(\frac{1}{\delta+m} + \frac{1}{\delta+d_m}\right)$$

(Equation 30)

To perform convenient simulations in cases with changeable inputs, we proposed another approximation, the step function approximation, and set $t = \frac{1}{2}T_1$ as the cut-off point:

$$f_2(t) = \begin{cases} 0 & t < T_2 \\ 1 & t \geq T_2 \end{cases} \qquad T_2 = \left(\frac{1}{\delta+m} + \frac{1}{\delta+d_m} \right) \tag{Equation 31}$$

Multistep regulation model

The input of the one-step regulation model was continuous and stable and did not change over time. However, in multistep regulation circuits, the expression levels of the intermediate regulatory proteins change over time. Therefore, the detailed model should be written as follows:

$$\frac{dR_Y}{dt} = b' + a' \frac{X^n(t)}{X^n(t)+K_X{}^n} - (\delta + d_m)R_Y$$

$$\frac{dU}{dt} = kR_Y - \delta U - mU \tag{Equation 32}$$

$$\frac{dY}{dt} = mU - \delta Y$$

where R_Y is the mRNA concentration, b' and a' are the basal and maximal transcription rates, K_X is the dissociation constant, n is the Hill coefficient, and d_m is the mRNA decay rate. Here, U is the unfolded protein, and Y is the folded (e.g., regulatory) or matured (e.g., fluorescent) protein, k is the translation rate, and m is the protein folding/maturation rate, and δ is the dilution rate due to cell division. The input $X(t)$ is the protein expression level over time, which controls the expression of protein Y.

Moreover, this detailed ODE model could be transformed into a third-order ODE as follows:

$$\frac{d^3Y}{dt^3} = mkb' + mka' \frac{X^n(t)}{X^n(t)+K_X{}^n} - (3\delta + d_m + m)\frac{d^2Y}{dt^2} - \left(3\delta^2 + 2\delta m + 2\delta d_m + md_m\right)\frac{dY}{dt} - \delta(\delta + m)(\delta + d_m)Y \tag{Equation 33}$$

$$\lambda_1 = -\delta, \lambda_2 = -(\delta + m), \lambda_3 = -(\delta + d_m) \tag{Equation 34}$$

Then, the equation of $Y(t)$ can be derived as follows:

$$Y(t) = \left(C_1 e^{-\delta t} + C_2 e^{-(\delta+m)t} + C_3 e^{-(\delta+d_m)} \right)$$

$$+ \frac{1}{md_m} e^{-\delta t} \int_0^t \left[mkb' + mka' \frac{X^n(t')}{X^n(t')+K_X{}^n} \right] e^{\delta t'} dt' - \frac{1}{m(d_m - m)} e^{-(\delta+m)t} \int_0^t \left[mkb' + mka' \frac{X^n(t')}{X^n(t')+K_X{}^n} \right] e^{(\delta+m)t'} dt'$$

$$+ \frac{1}{d_m(d_m - m)} e^{-(\delta+d_m)t} \int_0^t \left[mkb' + mka' \frac{X^n(t')}{X^n(t')+K_X{}^n} \right] e^{(\delta+d_m)t'} dt' \tag{Equation 35}$$

We can then obtain the following equation:

$$\frac{dY}{dt} + \delta Y = -C_2 m e^{-(\delta+m)t} - C_3 d_m e^{-(\delta+d_m)t} - \frac{mkb' e^{-(\delta+m)t}}{(\delta+m)(d_m - m)} + \frac{mkb' e^{-(\delta+d_m)t}}{(\delta+d_m)(d_m - m)} + \frac{mkb'}{(\delta+m)(\delta+d_m)}$$

$$+ \frac{mka'}{d_m - m} \left\{ e^{-(\delta+m)t} \int_0^t \frac{X^n(t')}{X^n(t')+K_X{}^n} e^{(\delta+m)t'} dt' - e^{-(\delta+d_m)t} \int_0^t \frac{X^n(t')}{X^n(t')+K_X{}^n} e^{(\delta+d_m)t'} dt' \right\} \tag{Equation 36}$$

The parameters can be derived according to the boundary conditions as follows:

$$C_1 = \frac{b}{\delta} - (C_2 + C_3), \qquad C_2 = \frac{-(\delta+d_m)b}{m(d_m - m)}, \qquad C_3 = \frac{(\delta+m)b}{d_m(d_m - m)} \tag{Equation 37}$$

$$a = \frac{mka'}{(\delta+m)(\delta+d_m)}, b = \frac{mkb'}{(\delta+m)(\delta+d_m)} \tag{Equation 38}$$

Then, the previous equation can be written as follows:

$$\frac{dY}{dt} + \delta Y = b + \frac{a(\delta+m)(\delta+d_m)}{d_m - m} \left\{ \int_0^t \frac{X^n(t')}{X^n(t')+K_X{}^n} e^{-(\delta+m)(t - t')} dt' \right.$$

$$\left. - \int_0^t \frac{X^n(t')}{X^n(t')+K_X{}^n} e^{-(\delta+d_m)(t - t')} dt' \right\} \tag{Equation 39}$$

By changing the variable $t' \rightarrow t - t'$, we obtain

$$\frac{dY}{dt} + \delta Y = b + \frac{a(\delta+m)(\delta+d_m)}{d_m - m} \left\{ \int_0^t \frac{X^n(t - t')}{X^n(t - t')+K_X^n} e^{-(\delta+m)t'} dt' \right.$$
$$\left. - \int_0^t \frac{X^n(t - t')}{X^n(t - t')+K_X^n} e^{-(\delta+d_m)t'} dt' \right\}$$

(Equation 40)

For brevity, we defined

$$Y_1(t) = \int_0^t \frac{X^n(t - t')}{X^n(t - t')+K_X^n} e^{-(\delta+m)t'} dt'$$

$$Y_2(t) = \int_0^t \frac{X^n(t - t')}{X^n(t - t')+K_X^n} e^{-(\delta+d_m)t'} dt'$$

(Equation 41)

$$Y_s(t) = \frac{X^n(t)}{X^n(t)+K_X^n}$$

We can then expand Y_s in a short time interval Δt:

$$Y_s(t + \Delta t) \approx Y_s(X(t)) + \left[Y_s'(X(t))\dot{X}(t) \right] \Delta t$$
$$+ \frac{1}{2} \left[Y_s''(X(t))\dot{X}^2(t) + Y_s'(X(t))\ddot{X}(t) \right] (\Delta t)^2$$

(Equation 42)

Then, we write Y_1 and Y_2 as follows[50]:

$$Y_1(t) = \int \left[Y_s(X(t)) + Y_s'(X(t))\dot{X}(t)(t' - t) \right] e^{-(\delta+m)(t - t')} dt = \frac{1}{\delta+m} Y_s(X(t)) \left(1 - e^{-(\delta+m)t} \right)$$
$$+ \frac{1}{\delta+m} Y_s'(X(t))\dot{X}(t) \left[te^{-(\delta+m)t} - \frac{1}{\delta+m} \left(1 - e^{-(\delta+m)t} \right) \right]$$

(Equation 43)

$$Y_2(t) = \int \left[Y_s(X(t)) + Y_s'(X(t))\dot{X}(t)(t' - t) \right] e^{-(\delta+d_m)(t - t')} dt' = \frac{1}{\delta+d_m} Y_s(X(t)) \left(1 - e^{-(\delta+d_m)t} \right)$$
$$+ \frac{1}{\delta+d_m} Y_s'(X(t))\dot{X}(t) \left[te^{-(\delta+d_m)t} - \frac{1}{\delta+d_m} \left(1 - e^{-(\delta+d_m)t} \right) \right]$$

(Equation 44)

Next, we derive the following equation[50]:

$$Y_1(t) - Y_2(t) = Y_s(X(t)) \left[\frac{1}{\delta+m} \left(1 - e^{-(\delta+m)t} \right) - \frac{1}{\delta+d_m} \left(1 - e^{-(\delta+d_m)t} \right) \right] + Y_s'(X(t))\dot{X}(t) \left[\frac{1}{\delta+m} te^{-(\delta+m)t} \right.$$
$$\left. - \frac{1}{\delta+d_m} te^{-(\delta+d_m)t} - \frac{1}{\delta+m^2} \left(1 - e^{-(\delta+m)t} \right) + \frac{1}{\delta+d_m^2} \left(1 - e^{-(\delta+d_m)t} \right) \right]$$

(Equation 45)

We define[50]

$$\omega = \frac{1}{\delta+m} \left(1 - e^{-(\delta+m)t} \right) - \frac{1}{\delta+d_m} \left(1 - e^{-(\delta+d_m)t} \right)$$

(Equation 46)

Then,

$$f(t - \tau_Y) = Y_s(X(t)) + Y_s'(X(t))\dot{X}(t)(- \tau_Y)$$
$$Y_1(t) - Y_2(t) \approx \omega f(t - \tau_Y) = \omega \left[Y_s(X(t)) + Y_s'(X(t))\dot{X}(t)(- \tau_Y) \right]$$
$$Y_1(t) - Y_2(t) \approx \omega Y_s(X((t - \tau_Y)))$$

(Equation 47)

$$\tau_Y \approx \left(\frac{1}{\delta+m} + \frac{1}{\delta+d_m} \right)$$
$$+ \frac{1}{d_m - m} \left((1 - (\delta + m)t)e^{-(\delta+d_m)t} - (1 - (\delta + d_m)t)e^{-(\delta+m)t} \right)$$

(Equation 48)

$$\tau_Y \approx \left(\frac{1}{\delta+m} + \frac{1}{\delta+d_m} \right)$$

(Equation 49)

Then, we finally derive:

$$\frac{dY}{dt} + \delta Y = b + a\left(1 + \frac{(\delta+m)e^{-(\delta+d_m)t} - (\delta+d_m)e^{-(\delta+m)t}}{d_m - m}\right)\frac{X^n(t - \tau_Y)}{X^n(t - \tau_Y)+K_X{}^n} \qquad \text{(Equation 50)}$$

$$f(t) = 1 + \frac{(\delta+m)e^{-(\delta+d_m)t} - (\delta+d_m)e^{-(\delta+m)t}}{d_m - m} \qquad \text{(Equation 51)}$$

Since we have proposed the step function approximation of $f(t)$ before, the characteristic delay time is $T_2 = \left(\frac{1}{\delta+m_Y} + \frac{1}{\delta+d_{m_Y}}\right)$, the same as τ_Y here, the final DDM can be written as follows:

$$\frac{dY}{dt} + \delta Y = b + a\frac{X^n(t - \tau_Y)}{X^n(t - \tau_Y)+K_X{}^n} \qquad \tau = \left(\frac{1}{\delta+m} + \frac{1}{\delta+d_m}\right) \qquad \text{(Equation 52)}$$

DDMs for different synthetic circuits

(1) The DDM of the cascaded three-step repression circuit can be formulated as follows:

$$\frac{dX_{T7}}{dt} = b_{lac} + a_{lac}\frac{\left(\frac{f_1}{K_{lac}}\right)^{n_{lac}}}{1+\left(\frac{f_1}{K_{lac}}\right)^{n_{lac}}} - \delta X_{T7} \qquad f_1 = \begin{cases} 0 & t < \tau_{T7} \\ \dfrac{[IPTG]^{n_{iptg}}}{[IPTG]^{n_{iptg}}+K_{IPTG}{}^{n_{iptg}}} & t \geq \tau_{T7} \end{cases}$$

$$\frac{dX_{CI434}}{dt} = b_{T7} + a_{T7}\frac{\left(\frac{X_{T7}(t - \tau_{CI434})}{K_{T7}}\right)^{n_{T7}}}{1+\left(\frac{X_{T7}(t - \tau_{CI434})}{K_{T7}}\right)^{n_{T7}}} - \delta X_{CI434} \qquad \text{(Equation 53)}$$

$$\frac{dX_{gfp}}{dt} = b_{CI434} + a_{CI434}\frac{1}{1+\left(\frac{X_{CI434}(t - \tau_{gfp})}{K_{CI434}}\right)^{n_{CI434}}} - \delta X_{gfp}$$

where b and a are the basal and maximum production rates of the protein, respectively, K is the dissociation constant, n is the Hill coefficient reflecting the cooperativity of the activators, δ is the dilution rate due to cell division, and τ is the characteristic delay time.

(2) The DDM of the IFFL type I circuit can be formulated as follows:

$$\frac{dX_{T7}}{dt} = b_{lac} + a_{lac}\frac{\left(\frac{f_1}{K_{lac}}\right)^{n_{lac}}}{1+\left(\frac{f_1}{K_{lac}}\right)^{n_{lac}}} - \delta X_{T7} \qquad f_1 = \begin{cases} 0 & t < \tau_{T7} \\ \dfrac{[IPTG]^{n_{iptg}}}{[IPTG]^{n_{iptg}}+K_{IPTG}{}^{n_{iptg}}} & t \geq \tau_{T7} \end{cases}$$

$$\frac{dX_{CI434}}{dt} = b_{lac} + a_{lac}\frac{\left(\frac{f_2}{K_{lac}}\right)^{n_{lac}}}{1+\left(\frac{f_2}{K_{lac}}\right)^{n_{lac}}} - \delta X_{CI434} \qquad f_2 = \begin{cases} 0 & t < \tau_{CI434} \\ \dfrac{[IPTG]^{n_{iptg}}}{[IPTG]^{n_{iptg}}+K_{IPTG}{}^{n_{iptg}}} & t \geq \tau_{CI434} \end{cases} \qquad \text{(Equation 54)}$$

$$\frac{dX_{gfp}}{dt} = b_{T7} + a_{T7}\frac{\left(\frac{X_{T7}(t - \tau_{gfp})}{K_{T7}}\right)^{n_{T7}}}{1+\left(\frac{X_{T7}(t - \tau_{gfp})}{K_{T7}}\right)^{n_{T7}}+\left(\frac{X_{CI434}(t - \tau_{gfp})}{K_{CI434}}\right)^{n_{CI434}}} - \delta X_{gfp}$$

where b and a are the basal and maximum production rates of the protein, respectively, K is the dissociation constant, n is the Hill coefficient reflecting the cooperativity of the activators, δ is the dilution rate due to cell division, and τ is the characteristic delay time.

(3) The DDM of the IFFL type II circuit can be formulated as follows:

$$\frac{dX_{T7}}{dt} = b_{lac} + a_{lac}\frac{\left(\frac{f_1}{K_{lac}}\right)^{n_{lac}}}{1+\left(\frac{f_1}{K_{lac}}\right)^{n_{lac}}} - \delta X_{T7} \qquad f_1 = \begin{cases} 0 & t < \tau_{T7} \\ \dfrac{[IPTG]^{n_{iptg}}}{[IPTG]^{n_{iptg}}+K_{IPTG}^{n_{iptg}}} & t \geq \tau_{T7} \end{cases}$$

$$\frac{dX_{CI434}}{dt} = b_{T7} + a_{T7}\frac{\left(\frac{X_{T7}(t - \tau_{CI434})}{K_{T7}}\right)^{n_{T7}}}{1+\left(\frac{X_{T7}(t - \tau_{CI434})}{K_{T7}}\right)^{n_{T7}}} - \delta X_{CI434} \qquad \text{(Equation 55)}$$

$$\frac{dX_{gfp}}{dt} = b_{T7} + a_{T7}\frac{\left(\frac{X_{T7}\left(t - \tau_{gfp}\right)}{K_{T7}}\right)^{n_{T7}}}{1+\left(\frac{X_{T7}\left(t - \tau_{gfp}\right)}{K_{T7}}\right)^{n_{T7}}+\left(\frac{X_{CI434}\left(t - \tau_{gfp}\right)}{K_{CI434}}\right)^{n_{CI434}}} - \delta X_{gfp}$$

where b and a are the basal and maximum production rates of the protein, respectively, K is the dissociation constant, n is the Hill coefficient reflecting the cooperativity of the activators, δ is the dilution rate due to cell division, and τ is the characteristic delay time.

QUANTIFICATION AND STATISTICAL ANALYSIS

Data are reported as mean +/− standard deviation (SD) from three experimental repeats. For each experiment, the results of at least 12 trap chamber repeats were averaged.